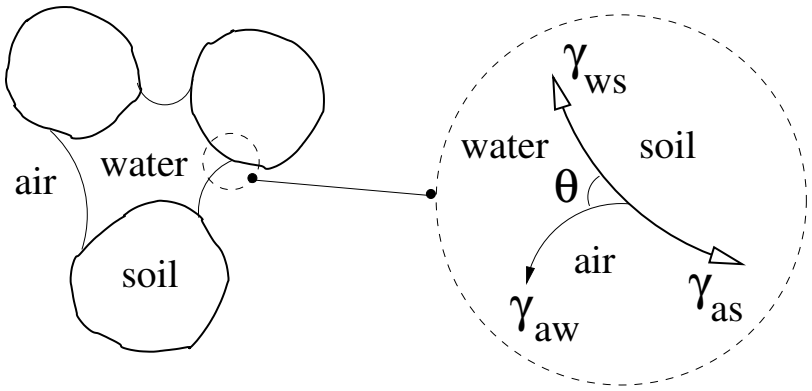

Figure 2.12: Configuration of air and water in pore space. The contact angle θ measured through the water is acute, so that water is the *wetting* phase. γ_{ws}, γ_{as} and γ_{aw} are the surface energies of the three interfaces.

interface is curved, and in an equilibrium configuration the curvature of this interface will be constant throughout the pore space. The value of the curvature depends on the amount of liquid present. The less liquid there is (i. e., the smaller the value of S), then the smaller the pores where the liquid is found, and thus the higher the curvature. Associated with the curvature is a suction effect due to surface tension across the air/water interface. The upshot of all this is that the air and water pressures are related by a *capillary suction characteristic* or *capillary pressure* function which expresses the difference between the pressures as a function of mean curvature, and hence, directly, S. Elementary geometry in a cylindrical pore of diameter d_p implies

$$p_a - p = \frac{2\gamma \cos\theta}{d_p}, \tag{2.121}$$

where θ is the contact angle. More generally, we can take

$$p_a - p = f(S). \tag{2.122}$$

The suction characteristic $f(S)$ is equal to $2\gamma\kappa$, where κ is the mean interfacial curvature: γ is the surface tension. For air and water in soil, f is positive as water is the *wetting phase*, that is, the *contact angle* at the contact line between air, water and soil grain is acute, measured through the water (see figure 2.12). The resulting form of $f(S)$ displays hysteresis as indicated in figure 2.13, with different curves depending on whether drying or wetting is taking place.

2.3.1 The Richards equation

To model the flow, we have the conservation of mass equation in the form

$$\frac{\partial(\phi S)}{\partial t} + \boldsymbol{\nabla}.\mathbf{u} = 0, \tag{2.123}$$

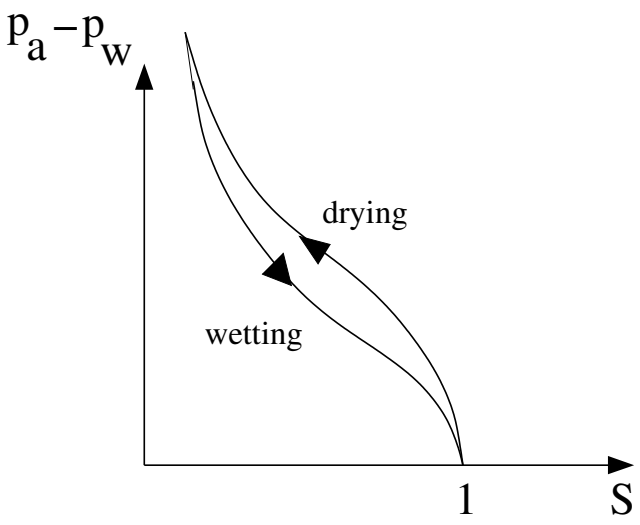

Figure 2.13: Capillary suction characteristic (A.K.A. capillary pressure). It displays hysteresis in wetting and drying.

where we take ϕ as constant. Darcy's law for an unsaturated flow has the form

$$\mathbf{u} = -\frac{k(S)}{\mu}[\boldsymbol{\nabla} p + \rho g \hat{\mathbf{k}}], \tag{2.124}$$

where the permeability k depends on S. If $k(1) = k_0$ (the saturated permeability), then one commonly writes $k = k_0 k_r(S)$, where k_r is the *relative permeability*. The most obvious assumption would be $k_r = S$, but this is rarely appropriate, and a better representation is a convex function, such as $k_r = S^3$. An even better representation is a function such as $k_r = \left(\frac{S - S_0}{1 - S_0}\right)_+^3$, where S_0 is known as the residual saturation. It represents the fact that in fine-grained soils, there is usually some minimal water fraction which cannot be removed. It is naturally associated with a capillary suction characteristic function $p_a - p = f(S)$ which tends to infinity as $S \to S_0+$, also appropriate for fine-grained soils.

In one dimension, and if we take the vertical coordinate (upwards) to be z, we obtain the *Richards equation*

$$\phi \frac{\partial S}{\partial t} - \frac{\partial V(S)}{\partial z} = \frac{\partial}{\partial z}\left[D(S)\frac{\partial S}{\partial z}\right], \tag{2.125}$$

where

$$V(S) = K_0 k_r(S), \quad D(S) = -\frac{K_0}{\rho g} k_r(S) f'(S), \quad K_0 = \frac{k_0 \rho g}{\mu}; \tag{2.126}$$

K_0 is the saturated hydraulic conductivity. We are assuming $p_a =$ constant (and also that the soil matrix is incompressible).

2.3.2 Non-dimensionalisation

We choose scales for the variables as follows:

$$f = p_e \psi, \quad z \sim l, \quad t \sim \frac{\phi l}{K_0}, \tag{2.127}$$

where we have defined the capillary pressure scale to be

$$p_e = \frac{\gamma}{d_p}; \tag{2.128}$$

here d_p is the (mean) pore diameter and γ is the surface tension, assumed constant. The quantity p_e is often referred to as the pore entry pressure, and we will discuss this in more detail later.

The Richards equation then becomes, in dimensionless variables,

$$S_t - k_r'(S) S_z = \varepsilon \left[D^*(S) S_z \right]_z, \tag{2.129}$$

where

$$D^*(S) = -k_r(S) \psi'(S). \tag{2.130}$$

Note that ψ is a decreasing function, so that the diffusion coefficient $D^* > 0$, as is indeed necessary. The single dimensionless parameter is

$$\varepsilon = \frac{p_e}{\rho g l}, \tag{2.131}$$

and is small for coarse soils, and $O(1)$ for fine-grained soils. As a specific example, we take $l = 1$ m, so that $\rho g l \sim 10^4$ Pa. If we take $\gamma = 70$ mN m^{-1} fpr water/air, and $d_p \sim 0.1$ mm, then $p_e \sim 700$ Pa, and $\varepsilon \sim 0.07$; this may be appropriate for sandy soils. For silty soils, we might have $d_p \sim 10$ μm, and then $\varepsilon \sim 0.7$.

As a specific example, we consider the case of soil wetting due to surface infiltration: of rainfall, for example. Suppose that there is a constant downwards flux of (dimensional) rainfall q at the surface. It is convenient to define the depth $\zeta = -z$, and take the vadose zone to be in $0 < \zeta < 1$. The Richards equation is then

$$S_t + k_r'(S) S_\zeta = \varepsilon \left[D^*(S) S_\zeta \right]_\zeta, \tag{2.132}$$

and suitable boundary conditions for the saturation are

$$\begin{aligned} k_r(S) - \varepsilon D^*(S) S_\zeta &= q^* \quad \text{at} \quad \zeta = 0, \quad q^* = \frac{q}{K_0}, \\ S &= 1 \quad \text{at} \quad \zeta = 1. \end{aligned} \tag{2.133}$$

In the steady state, the first condition in (2.133) applies everywhere, and the solution is a quadrature,

$$\int_S^1 \frac{\varepsilon D^*(S)\, dS}{k_r(S) - q^*} = 1 - \zeta. \tag{2.134}$$

Obviously S must be an increasing function of ζ, and this requires $q^* < k_r(1) = 1$, in other words $q < K_0$: the supplied rainfall must be less than the saturated hydraulic conductivity.

What if it is not? It is easy to see from the solution (2.134) that as $q^* \to 1-$, the saturation approaches one. If $q > K_0$, the supplied flux at the surface is greater than the soil's maximum drainage capacity (which is the saturated hydraulic conductivity). So in this case, water must pond at the surface, and the boundary condition is replaced by $S = 1$ at $\zeta = 0$; clearly in this case, the soil is waterlogged and the water table is pushed up to the soil surface. Such ponding is commonly observed during periods of heavy rainfall. For silt with $k_0 = 10^{-14}$ m^2, the hydraulic conductivity $K_0 \sim 10^{-7}$ m s^{-1} or 3 m y^{-1}, while average rainfall in England, for example, is ≤ 1 m y^{-1}. Thus *on average* $q^* \leq 1$ for such soils, but during storms we can expect $q^* \gg 1$. When ponding does occur, the pond depth is determined by the balance between precipitation, infiltration, and surface run-off.

2.3.3 Snow melting

An application of the unsaturated flow model occurs in the study of melting snow. In particular, it is found that pollutants which may be uniformly distributed in snow (e. g. sulphate SO_4^{2-} from sulphur emissions via acid rain) can be concentrated in melt water run-off, with a consequent enhanced detrimental effect on stream pollution. The question then arises, why this should be so? We shall find that uniform surface melting of a dry snowpack can lead to a meltwater spike at depth.

Suppose we have a snow pack of depth l. Snow is a porous aggregate of ice crystals, and meltwater formed at the surface can percolate through the snow pack to the base, where run-off occurs. (We ignore effects of re-freezing of meltwater.) The model (2.132) is appropriate, and to be specific, we will also take

$$k_r = S^3, \quad \psi(S) = \frac{1}{S} - S, \tag{2.135}$$

based on typical experimental results.

Suitable boundary conditions in a melting event might be to prescribe the melt flux q_0 at the surface, thus

$$k_r \left(\varepsilon \frac{\partial \psi}{\partial \zeta} + 1 \right) = q^* = \frac{q_0}{K_0} \quad \text{at} \quad \zeta = 0. \tag{2.136}$$

If the base is impermeable, then

$$k_r \left(\varepsilon \frac{\partial \psi}{\partial \zeta} + 1 \right) = 0 \ \text{ at } \ \zeta = 1. \tag{2.137}$$

This is certainly not realistic if S reaches 1 at the base, since then ponding must occur and presumably melt drainage will occur via a sub-horizontal flow under the snowpack, but we will examine the initial stages of the flow using (2.137) before that

happens. Finally, we suppose $S = 0$ at $t = 0$. Again, this is not realistic in the model (it implies infinite capillary suction) but it is a feasible approximation to make.

Simplification of this model now leads to the dimensionless Richards equation in the form

$$\frac{\partial S}{\partial t} + 3S^2\frac{\partial S}{\partial \zeta} = \varepsilon\frac{\partial}{\partial \zeta}\left[S(1+S^2)\frac{\partial S}{\partial \zeta}\right]. \tag{2.138}$$

If we choose $\gamma = 70$ mN m^{-1}, $d_p = 0.1$ mm, $\rho = 10^3$ kg m^{-3}, $g = 10$ m s^{-2}, $l = 1$ m as before, then again $\varepsilon = 0.07$. It follows that (2.138) has a propensity to form shocks, these being diffused by the term in ε over a distance $O(\varepsilon)$ (by analogy with the shock structure for the Burgers equation).

We want to solve (2.138) with the initial condition

$$S = 0 \quad \text{at} \quad t = 0, \tag{2.139}$$

and the boundary conditions

$$S^3 - \varepsilon S(1+S^2)\frac{\partial S}{\partial \zeta} = q^* \quad \text{on} \quad \zeta = 0, \tag{2.140}$$

and

$$S^3 - \varepsilon S(1+S^2)\frac{\partial S}{\partial \zeta} = 0 \quad \text{at} \quad \zeta = 1. \tag{2.141}$$

Roughly, for $\varepsilon \ll 1$, these are

$$\begin{aligned} S &= S_0 \quad \text{at} \quad \zeta = 0, \\ S &= 0 \quad \text{at} \quad \zeta = 1, \end{aligned} \tag{2.142}$$

where $S_0 = q^{*1/3}$, which we initially take to be $O(1)$ (and < 1, so that surface ponding does not occur).

Neglecting ε, the solution is the step function

$$\begin{aligned} S &= S_0, \qquad \zeta < \zeta_f, \\ S &= 0, \qquad \zeta > \zeta_f, \end{aligned} \tag{2.143}$$

and the shock front at ζ_f advances at a rate $\dot{\zeta}_f$ given by the jump condition

$$\dot{\zeta}_f = \frac{[S^3]^+_-}{[S]^+_-} = S_0^2. \tag{2.144}$$

In dimensional terms, the shock front moves at speed $q_0/\phi S_0$, which is in fact obvious (given that it has constant S behind it).

The shock structure is similar to that of Burgers' equation. We put

$$\zeta = \zeta_f + \varepsilon Z, \tag{2.145}$$

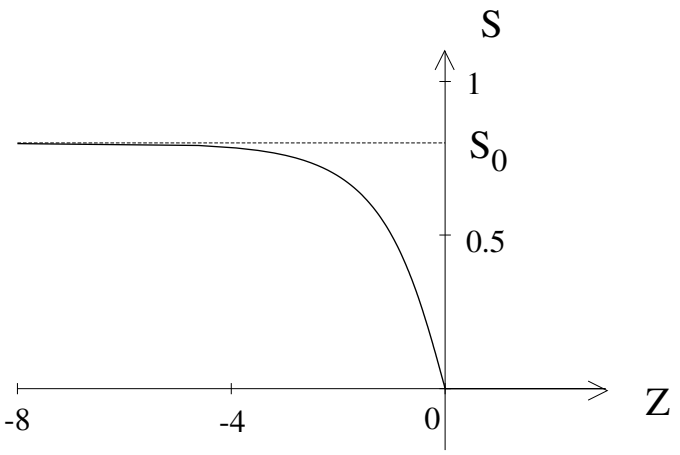

Figure 2.14: $S(Z)$ given by (2.150); the shock front terminates at the origin.

and S rapidly approaches the quasi-steady solution $S(Z)$ of

$$-cS' + 3S^2S' = [S(1+S^2)S']', \tag{2.146}$$

where $c = \dot{\zeta}_f$; hence

$$S(1+S^2)S' = -S(S_0^2 - S^2), \tag{2.147}$$

in order that $S \to S_0$ as $Z \to -\infty$, and where we have chosen

$$c = S_0^2, \tag{2.148}$$

(as $S_+ = 0$), thus reproducing (2.144). The solution is a quadrature,

$$\int^S \frac{(1+S^2)\,dS}{(S_0^2 - S^2)} = -Z, \tag{2.149}$$

with an arbitrary added constant (amounting to an origin shift for Z). Hence

$$S - \frac{(1+S_0^2)}{2S_0} \ln\left[\frac{S_0+S}{S_0-S}\right] = Z. \tag{2.150}$$

The shock structure is shown in figure 2.14; the profile terminates where $S = 0$ at $Z = 0$. In fact, (2.147) implies that $S = 0$ or (2.150) applies. Thus when S given by (2.150) reaches zero, the solution switches to $S = 0$. The fact that $\partial S/\partial Z$ is discontinuous is not a problem because the diffusivity $S(1+S^2)$ goes to zero when $S = 0$. This degeneracy of the equation is a signpost for fronts with discontinuous derivatives: essentially, the profile can maintain discontinuous gradients at $S = 0$ because the diffusivity is zero there, and there is no mechanism to smooth the jump away.

Suppose now that $k_0 = 10^{-10}$ m^2 and $\mu/\rho = 10^{-6}$ m^2 s^{-1}; then the saturated hydraulic conductivity $K_0 = k_0\rho g/\mu = 10^{-3}$ m s^{-1}. On the other hand, if a metre

thick snow pack melts in ten days, this implies $q_0 \sim 10^{-6}$ m s^{-1}. Thus $S_0^3 = q_0/K_0 \sim 10^{-3}$, and the approximation $S \approx S_0$ looks less realistic. With

$$S^3 - \varepsilon S(1+S^2)\frac{\partial S}{\partial \zeta} = S_0^3, \tag{2.151}$$

and $S_0 \sim 10^{-1}$ and $\varepsilon \sim 10^{-1}$, it seems that one should assume $S \ll 1$. We define

$$S = \left(\frac{S_0^3}{\varepsilon}\right)^{1/2} s; \tag{2.152}$$

(2.151) becomes

$$\beta s^3 - s\left[1 + \frac{S_0^3}{\varepsilon}s^2\right]\frac{\partial s}{\partial \zeta} = 1 \quad \text{on} \quad \zeta = 0, \tag{2.153}$$

and we have $S_0^3/\varepsilon \sim 10^{-2}$, $\beta = (S_0/\varepsilon)^{3/2} \sim 1$.

We neglect the term in S_0^3/ε, so that

$$\beta s^3 - s\frac{\partial s}{\partial \zeta} \approx 1 \quad \text{on} \quad \zeta = 0, \tag{2.154}$$

and substituting (2.152) into (2.138) leads to

$$\frac{\partial s}{\partial \tau} + 3\beta s^2 \frac{\partial s}{\partial \zeta} \approx \frac{\partial}{\partial \zeta}\left[s\frac{\partial s}{\partial \zeta}\right], \tag{2.155}$$

if we define $t = \tau/\left(\varepsilon S_0^3\right)^{1/2}$. A simple analytic solution is no longer possible, but the development of the solution will be similar. The flux condition (2.154) at $\zeta = 0$ allows the surface saturation to build up gradually, and a shock will only form if $\beta \gg 1$ (when the preceding solution becomes valid).

2.3.4 Similarity solutions

If, on the other hand, $\beta \ll 1$, then the saturation profile approximately satisfies

$$\begin{aligned} \frac{\partial s}{\partial \tau} &= \frac{\partial}{\partial \zeta}\left[s\frac{\partial s}{\partial \zeta}\right], \\ -s\frac{\partial s}{\partial \zeta} &= \begin{cases} 1 & \text{on} \quad \zeta = 0, \\ 0 & \text{on} \quad \zeta = 1. \end{cases} \end{aligned} \tag{2.156}$$

At least for small times, the model admits a similarity solution of the form

$$s = \tau^\alpha f(\eta), \quad \eta = \zeta/\tau^\beta, \tag{2.157}$$

where satisfaction of the equations and boundary conditions requires $2\alpha = \beta$ and $2\beta = 1 = \alpha$, whence $\alpha = \frac{1}{3}$, $\beta = \frac{2}{3}$, and f satisfies

$$(ff')' - \tfrac{1}{3}(f - 2\eta f') = 0, \tag{2.158}$$

with the condition at $\zeta = 0$ becoming

$$-ff' = 1 \quad \text{at} \quad \eta = 0. \tag{2.159}$$

The condition at $\zeta = 1$ can be satisfied for small enough τ, as we shall see, because the equation (2.158) is degenerate, and f reaches zero in a finite distance, η_0, say, and $f = 0$ for $\eta > \eta_0$. As $\eta = 1/\tau^{2/3}$ at $\zeta = 1$, then this solution will satisfy the no flux condition at $\zeta = 1$ as long as $\tau < \eta_0^{-3/2}$, when the advancing front will reach $\zeta = 1$.

To see why f behaves in this way, integrate once to find

$$f(f' + \tfrac{2}{3}\eta) = -1 + \int_0^\eta f \, d\eta. \tag{2.160}$$

For small η, the right hand side is negative, and f is positive (to make physical sense), so f decreases (and in fact $f' < -\frac{2}{3}\eta$). For sufficiently small $f(0) = f_0$, f will reach zero at a finite distance $\eta = \eta_0$, and the solution must terminate. On the other hand, for sufficiently large f_0, $\displaystyle\int_0^\eta f \, d\eta$ reaches 1 at $\eta = \eta_1$ while f is still positive (and $f' = -\frac{2}{3}\eta_1$ there). For $\eta > \eta_1$, then f remains positive and $f' > -\frac{2}{3}\eta$ (f cannot reach zero for $\eta > \eta_1$ since $\displaystyle\int_0^\eta f \, d\eta > 1$ for $\eta > \eta_1$). Eventually f must have a minimum and thereafter increase with η. This is also unphysical, so we require f to reach zero at $\eta = \eta_0$. This will occur for a range of f_0, and we have to select f_0 in order that

$$\int_0^{\eta_0} f \, d\eta = 1, \tag{2.161}$$

which in fact represents global conservation of mass. Figure 2.15 shows the schematic form of solution both for $\beta \gg 1$ and $\beta \ll 1$. Evidently the solution for $\beta \sim 1$ will have a profile with a travelling front between these two end cases.

2.4 Immiscible two-phase flows

In some circumstances, the flow of more than one phase in a porous medium is important. For example, the flow of CO_2 in water (carbon sequestration), or the flow of oil and gas, or oil and water (or all three!) in a sedimentary basin, such as that beneath the North Sea. Suppose there are two phases; denote the phases by subscripts w and n, being the *wetting* and *non-wetting* fluids, and S_w, S_n are the saturations. It is assumed that together these two phases occupy all the pore space, such that $S_n + S_w = 1$. Note that the definition of which fluid is wetting and which is non-wetting relates to the size of the contact angle between the phases (i.e. if the angle is less than $\pi/2$, the fluid is known as wetting).

For each phase, there is an associated relative permeability function, which we denote $k_{rn}(S_n)$ and $k_{rw}(S_n)$. We write these in terms of the non-wetting saturation without loss of generality (since $S_w = 1 - S_n$). As discussed before, k_{rn} is a monotone

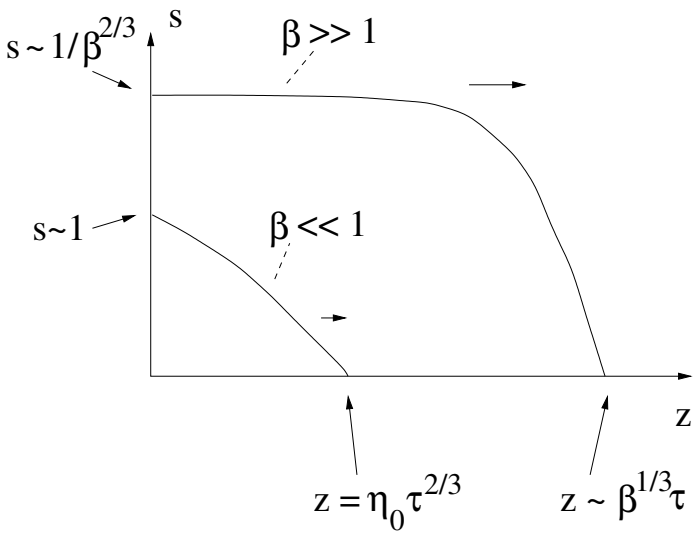

Figure 2.15: Schematic representation of the evolution of s in (2.155) for both large and small β.

increasing function of S_n, and for the same reasons k_{rw} is a decreasing function of S_n. They do not necessarily have a similar functional form. Furthermore, they typically display hysteresis phenomena. For example, it is easier (i.e. larger relative permeability) for CO_2 to invade a region of pore space than it is for it to withdraw from an existing area. This is the chief mechanism for capillary trapping during carbon sequestration.

The capillary (or suction) pressure $p_c = p_n - p_w$ is given by

$$p_c(S_n) = p_e \psi(S_n), \tag{2.162}$$

where p_e is the pore entry pressure, and ψ is a positive, monotonically increasing function of saturation S_n. The pore entry pressure is the minimum pressure required to fill the largest pore spaces of the rock with non-wetting phase. As the difference in pressure $p_n - p_w$ increases, smaller and smaller pore spaces can be occupied with non-wetting phase.

Mass conservation takes the form

$$\begin{aligned} \phi \frac{\partial S_n}{\partial t} + \boldsymbol{\nabla}.\mathbf{u}_n &= 0, \\ \phi \frac{\partial S_w}{\partial t} + \boldsymbol{\nabla}.\mathbf{u}_w &= 0, \end{aligned} \tag{2.163}$$

where ϕ is (constant) porosity, and Darcy's law for each phase is

$$\begin{aligned} \mathbf{u}_n &= -\frac{k_0}{\mu_n} k_{rn}(S_n) \left[\boldsymbol{\nabla} p_n + \rho_n g \hat{\mathbf{k}} \right], \\ \mathbf{u}_w &= -\frac{k_0}{\mu_w} k_{rw}(S_n) \left[\boldsymbol{\nabla} p_w + \rho_w g \hat{\mathbf{k}} \right]. \end{aligned} \tag{2.164}$$

2.4.1 Buckley-Leverett Flow

A canonical case of two-phase flow in porous media is the study of immiscible displacement in a long-thin aquifer, also known as Buckley-Leverett flow. To model this, we make the assumption that the flow is approximately one-dimensional, and the effects of gravity can be ignored. Such flows are relevant to geothermal energy production and carbon sequestration, but the problem formulation was originally employed to model hydrocarbon extraction in geological reservoirs.

We consider a constant injection of wetting and non-wetting phases at the aquifer inlet $x = 0$, and model the spatial and temporal development of the saturations S_n, S_w, downstream towards the aquifer outlet at $x = L$ (see figure 2.16). By conservation of mass (2.163) we have

$$u_n + u_w = U, \tag{2.165}$$

for some constant inlet velocity U. By inserting (2.164) (in one dimension) into (2.165) and substituting $p_w = p_n - p_c$, we get

$$-\frac{k_0}{\mu_w}\left[Mk_{rn}\frac{\partial p_n}{\partial x} + k_{rw}\left(\frac{\partial p_n}{\partial x} - \frac{\partial p_c}{\partial x}\right)\right] = U, \tag{2.166}$$

where $M = \mu_w/\mu_n$ is the viscosity ratio. Hence, we can re-arrange to get the non-wetting pressure gradient,

$$\frac{\partial p_n}{\partial x} = \frac{-\mu_w U/k_0}{Mk_{rn} + krw} + \frac{k_{rw}}{Mk_{rn} + k_{rw}}\frac{\partial p_c}{\partial x}. \tag{2.167}$$

By inserting this into (2.163) we get the governing equation for the saturation

$$\phi\frac{\partial S_n}{\partial t} + V(S_n)\frac{\partial S_n}{\partial x} = \frac{\partial}{\partial x}\left[D(S_n)\frac{\partial S_n}{\partial x}\right], \tag{2.168}$$

where the functions V, D are defined as

$$\begin{aligned} V(S_n) &= U\frac{\partial}{\partial S_n}\left[\frac{Mk_{rn}}{Mk_{rn} + k_{rw}}\right], \\ D(S_n) &= \frac{k_0 p_e}{\mu_w}\frac{Mk_{rn}k_{rw}}{Mk_{rn} + k_{rw}}\frac{\partial \psi}{\partial S_n}. \end{aligned} \tag{2.169}$$

The second term in (2.168) can therefore be interpreted as advection at speed $V = UJ'(S_n)$, where $J = Mk_{rn}/(Mk_{rn} + k_{rw})$ is the flow rate fraction. The third term is diffusive, indicating that the role of the capillary pressure is to smooth out gradients in the saturation S_n. It should be noted that a similar formulation can be achieved in terms of S_w, but here we stick with an S_n formulation without loss of generality.

It is interesting to measure the relative importance between each of these advective and diffusive effects. For this, we define a dimensionless Peclet number,

$$\mathrm{Pe} = \frac{U\mu_w L}{k_0 p_e}. \tag{2.170}$$

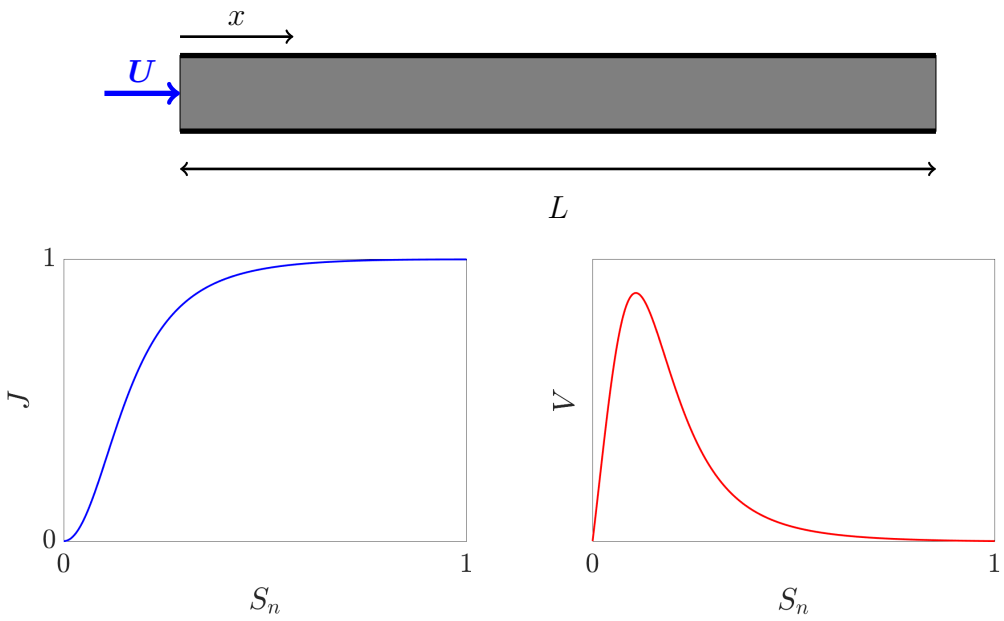

Figure 2.16: Schematic diagram and plots of the dimensionless flow rate fraction $J(S)$ and advection speed $V(S)$ as a function of non-wetting fluid saturation S_n (for the Buckley-Leverett problem). The viscosity ratio M is taken to be 30.

In many environmental scenarios, the above parameters lead to a large Peclet number $\mathrm{Pe} \gg 1$, such that the effects of diffusion (and hence the third term in (2.168)) can be ignored to good approximation. This approximation breaks down, however, when there are sharp gradients of S_n, such as near a shock. In such scenarios where there are shocks, one can introduce a boundary layer near the shock front to address diffusive effects.

By non-dimensionalising the model according to

$$x \sim L, \quad t \sim \phi L/U, \quad V \sim U, \tag{2.171}$$

and by dropping the subscript $S = S_n$, we get the simple advection equation

$$S_t + V(S)S_x = 0. \tag{2.172}$$

Such equations can be solved using the method of characteristics

$$\frac{\mathrm{d}x}{\mathrm{d}t} = V(S), \tag{2.173}$$

given suitable inlet and initial conditions at $x = 0$ and $t = 0$. As an example we consider the initial/boundary conditions

$$\begin{aligned} S(0,t) &= 1, \\ S(x,0) &= 0. \end{aligned} \tag{2.174}$$

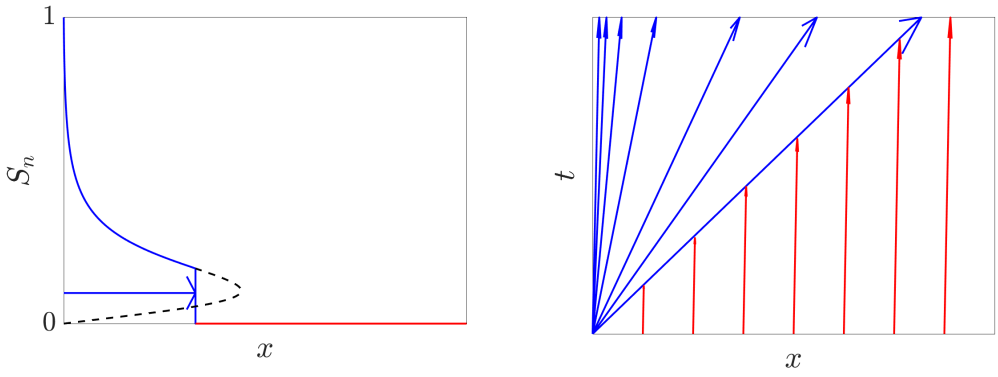

Figure 2.17: Illustration of a shock developing during Buckley-Leverett flow, as well as the corresponding characteristics in the $x-t$ plane. Blue curves indicate $S_n > S_s$ and red curves indicate $S_n = 0$.

This corresponds to an aquifer which is initially saturated with wetting phase, at which point pure non-wetting phase is injected at the inlet (e.g. CO_2 injected into a brine-filled aquifer).

To address this case, we first need to define expressions for the relative permeability functions in the advection term $V(S)$. For this we use the so-called 'Corey' model,

$$k_{rn} = S^{\alpha}, \quad k_{rw} = (1-S)^{\beta}, \tag{2.175}$$

where $\alpha, \beta > 0$ are some empirical constants. In this case, plots of the flow rate fraction J and advection speed V are shown in figure 2.16 for illustration. In general, J is a monotone increasing function between 0 and 1 (reminiscent of a CDF for example), whereas V is a positive function with a unique maximum.

The non-monotone behaviour of V in conjunction with (2.173)-(2.174) indicate that a shock will develop to maintain a saturation S that is not multi-valued. To determine the saturation value at the shock, we employ the Rankine-Hugoniot jump condition, which takes the form

$$\frac{\mathrm{d}x}{\mathrm{d}t} = \frac{[Q]^+_-}{[P]^+_-}, \tag{2.176}$$

for a PDE of the form $P_t + Q_x = 0$. Hence, we have the shock condition

$$V(S_s)S_s = J(S_s), \tag{2.177}$$

which must be solved to find S_s.

A typical shock solution is displayed in figure 2.17 together with characteristics in the $x-t$ plane. Clearly the shock at $S = S_s$ causes the characteristics from $t = 0$ to collide with the dividing characteristic $X(t) = V(S_s)t$. As described earlier, diffusive effects due to the capillary pressure act to smooth out this shock front. This occurs over a boundary layer of width $\delta \propto (t/\mathrm{Pe})^{1/2}$, located near the shock front $X(t)$.

2.4.2 Two-phase flow in heterogeneous media

Earlier we described how heterogeneities can affect the flow of a single phase within a porous medium. Here, we extend this analysis to account for multiphase effects between immiscible flows. In our earlier analysis, we discussed how heterogeneities are often characterised by variations in the pore size within a rock, manifesting in non-uniform porosity and permeability ϕ, k. However, variations in the pore size are also associated with different pore entry pressures p_e and therefore non-uniform capillary pressure p_c. In this section we describe how such variations modify the flow and distribution of the phase saturations S_n, S_w.

As before, it is useful to consider the most simple type of heterogeneity to gain a general understanding of the typical behaviour. To do so, we consider flow parallel to a system of two layers of equal thickness with permeability, porosity and pore entry pressure values k_i, ϕ_i, p_{e_i}, for $i = 1, 2$. The length and thickness of the medium is given by L, H, and the flow is predominantly horizontal, driven by an overarching pressure gradient $\Delta p/L$ (e.g. in the non-wetting phase).

It is useful to characterise the relative importance of viscous and capillary effects by the ratio

$$\frac{\partial p_n/\partial x}{\partial p_c/\partial z} \approx \frac{\Delta p/L}{\Delta p_e/H}, \tag{2.178}$$

where $\Delta p_e = p_{e_1} - p_{e_2}$. The above expression is the ratio between horizontal viscous pressure gradients and vertical gradients in the capillary pressure. We see this is analogous to the capillary number described earlier (remember $\mathrm{Ca} \sim \mu U/\gamma$). Hence, we write

$$\mathrm{Ca} = 1/\Gamma = \left| \frac{\Delta p H}{\Delta p_e L} \right|, \tag{2.179}$$

where a modulus sign is included to make sure the quantity is always positive, and Γ is introduced as a more intuitive alternative to the capillary number (since large Γ corresponds with large capillary effects).

The limit of large Γ is known as the "capillary limit". In this case the saturation of phases is dominated by capillary forces. Essentially, surface tension drives non-wetting phase into regions of larger pore space and away from smaller pore space (i.e. minimising surface energy). Comparatively the horizontal, viscous flow of phases is of lesser importance than the lateral rearrangement due to capillary effects.

By contrast, the limit of small Γ is known as the "viscous limit". In this case, the effect of capillary forces is negligible, and instead the flow is dominated by the flow-driving horizontal pressure gradients associated with viscous resistance. There is little saturation rearrangement due to surface tension, so the lateral saturation distribution remains close to the inlet conditions.

In general to account for the flow in such scenarios, we would have to solve the governing equations (2.163)-(2.164) for fixed Γ and suitable boundary conditions. However, in the limit of small and large Γ, we can make some simplifying assumptions to derive analytical solutions which give insight into the problem.

To start with we consider the case of steady flow in the viscous limit ($\Gamma \ll 1$). In this case, it can be shown (via asymptotic analysis) that the saturation is spatially uniform, e.g. $S_n = \bar{S}_n = S_n(x = 0)$. In other words, the saturation of phases remains the same as imposed at the inlet $x = 0$. Hence, the flow of non-wetting phase (for example) is

$$u_n = -\frac{k(z)}{\mu_n} k_{rn}(S_n) \frac{\partial p_n}{\partial x} = -\frac{k(z)}{\mu_n} k_{rn}(\bar{S}_n) \frac{\Delta p}{L}. \tag{2.180}$$

Hence, we can derive an effective property for the relative permeabilities in the viscous limit

$$\begin{aligned} k^V_{rn}(\bar{S}_n) &= \frac{\mu_n \bar{u}_n L}{-\Delta p \bar{k}} = k_{rn}(\bar{S}_n), \\ k^V_{rw}(\bar{S}_n) &= \frac{\mu_w \bar{u}_w L}{-\Delta p \bar{k}} = k_{rw}(\bar{S}_n), \end{aligned} \tag{2.181}$$

where bars indicate vertical averaging (e.g. $\bar{k} = (k_1 + k_2)/2$ for even thickness layers). These effective properties tell us how the mean flow $\bar{u}_n$, $\bar{u}_w$ depends on the mean saturation, permeability, and viscous pressure gradient. Hence, if we know information about the heterogeneity, we can immediately describe the flow in the viscous limit without doing any intensive computations.

Similarly, in the capillary limit ($\Gamma \gg 1$) we can derive analogous effective properties. In this case, the flow is associated with very weak driving pressure gradients $\Delta p/L$. Hence, p_n and p_w are expected to be approximately constant. This leads to a capillary pressure

$$p_c = p_n - p_w \approx \gamma, \tag{2.182}$$

for some constant γ. The capillary pressure is related to the saturation according to (2.162), given some model for p_c. For this, we employ the commonly used Brooks-Corey model, which is

$$p_c(S_n) = p_e(z)(1 - S_n)^{-1/\lambda}, \tag{2.183}$$

where λ represents the pore size distribution (large/small values of λ correspond with a large/small distribution of pore sizes). Inverting this function we get

$$S_n(z) = 1 - \left(\frac{p_e(z)}{\gamma}\right)^{\lambda}. \tag{2.184}$$

This can be re-written in terms of the average (i.e. removing γ) as

$$S_n(z) = 1 - \frac{p_e(z)^{\lambda}}{\overline{p_e^{\lambda}}}(1 - \bar{S}_n). \tag{2.185}$$

Hence, we can insert this into the Darcy equations and take the average, giving

$$\bar{u}_n = -\frac{1}{\mu_n} \overline{k(z) k_{rn}(S_n(z))} \frac{\Delta p}{L}. \tag{2.186}$$

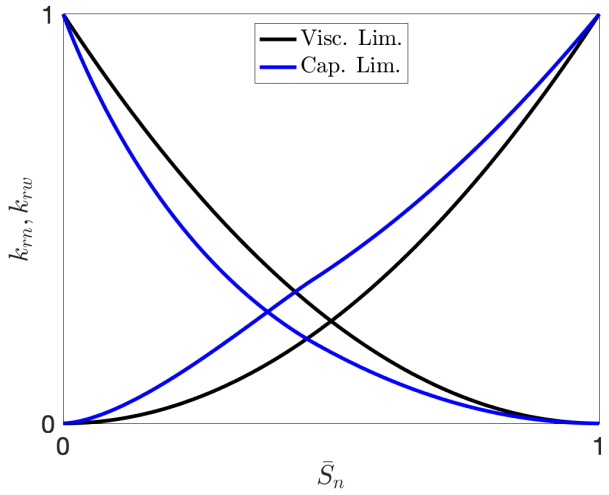

Figure 2.18: Effective relative permeabilities in the viscous and capillary limits in the case of flow parallel to a layered heterogeneous porous medium.

This (and a similar expression for the wetting phase) can be rearranged to derive expressions for effective relative permeabilities in the capillary limit, which are

$$\begin{aligned} k_{rn}^C(\bar{S}_n) &= \frac{\mu_n \bar{u}_n L}{-\Delta p \bar{k}} = \frac{\overline{k k_{rn}}}{\bar{k}}, \\ k_{rw}^C(\bar{S}_n) &= \frac{\mu_w \bar{u}_w L}{-\Delta p \bar{k}} = \frac{\overline{k k_{rw}}}{\bar{k}}. \end{aligned} \tag{2.187}$$

Hence, we now have sufficient information to describe the bulk flow through a heterogeneous aquifer in the limit of small and large Γ without having do to any intensive computations. These two cases are the two end members (extreme scenarios) and therefore provide upper and lower bounds for the general case of $\Gamma = \mathcal{O}(1)$.

Due to the form of (2.184), capillary forces act to push non-wetting phase into regions of smaller p_e, which corresponds with larger pore space and larger values of k, ϕ. Hence, non-wetting phase is preferentially rearranged into less resistive channels of flow, enhancing $\bar{u}_n$ and reducing $\bar{u}_w$. In this way, the effective relative permeabilities usually satisfy

$$k_{rn}^C > k_{rn}^V, \quad k_{rw}^C < k_{rw}^V. \tag{2.188}$$

In other words, heterogeneities act to enhance the flow of non-wetting phase and decrease the flow of wetting phase, which is in very good agreement with observations. An example of these effective properties is illustrated in figure 2.18. We will explore an example of such flows in Problem Sheet 3.

2.4.3 Heterogeneous Buckley-Leverett flows

The Buckley-Leverett flow studied earlier can be easily extended to account for heterogeneous systems. Whilst the flow formulation is in one-dimension, we can account for a vertical heterogeneity (i.e. sedimentary layers in two or three dimensions) by using effective properties for the relative permeabilities, either in the viscous or capillary limits. Hence, this models the vertical rearrangement of saturation due to capillary forces in a very long-thin aquifer in which the flow is predominantly one-dimensional.

As such, we can write down a dimensionless advection equation for the saturation of non-wetting phase

$$S_t + V(S)S_x = 0, \tag{2.189}$$

where the advection speed is given by either the capillary or viscous limits

$$V = \begin{cases} V^V(S), & \text{using} \quad k^V_{rn}, k^V_{rw} : \quad \Gamma \gg 1, \\ V^C(S), & \text{using} \quad k^C_{rn}, k^C_{rw} : \quad \Gamma \ll 1. \end{cases} \tag{2.190}$$

It should be noted that both the capillary and viscous limits have different shock saturation values S_s and consequently different advection speeds. Typically, since the flow of non-wetting phase is enhanced by heterogeneities, the capillary limit speed is usually faster than the viscous limit speed, such that $V^C(S_s) > V^V(S_s)$.

This class of approaches is sometimes referred to as 'upscaling', since the effects of the small-scale heterogeneities are incorporated into a model which describes the large-scale flow. Upscaling is useful in many environmental applications since it is much more computationally efficient than direct simulation, and also allows for ensemble predictions or best/worst case scenario estimates. Time-dependent simulation of a three-dimensional reservoir incorporating heterogeneities from the mm scale up to the km scale is not tractable. This is not only a result of computational limitations, but also due to a lack of existing heterogeneity data. For example, seismic surveys usually have a resolution of around $\sim$1 m.

2.4.4 Incorporating gravity

Let's consider the two-phase analogy of a gravity current spreading beneath an impermeable cap rock. For example, in the context of carbon sequestration, CO_2 is the non-wetting phase and salty brine is the wetting phase. As before, we assume that the flow has a long-thin aspect ratio. As a result, both the non-wetting and wetting phases satisfy a hydrostatic balance at leading order, such that

$$\begin{aligned} \frac{\partial p_n}{\partial z} &= \rho_n g, \\ \frac{\partial p_w}{\partial z} &= \rho_w g. \end{aligned} \tag{2.191}$$

This indicates that the capillary pressure satisfies

$$\frac{\partial p_c}{\partial z} = -\Delta\rho g. \tag{2.192}$$

Hence, in the absence of heterogeneity we have

$$p_c = p_e - \Delta\rho g(z - h), \tag{2.193}$$

where $z = h(x, t)$ is the gravity current thickness (measured downwards from the cap rock at $z = 0$). Hence, the capillary pressure can be inverted for the saturation of non-wetting phase,

$$S_n = 1 - (1 + \mathrm{Bo}(h/L - z/L))^{-\lambda}, \tag{2.194}$$

where $\mathrm{Bo} = \Delta\rho g L/p_e$ is the Bond number. The above expression is known as the 'gravity-capillary' balance. Hence, given a thickness h and Bond number, we can now calculate the vertical saturation distribution. In particular, S_n increases vertically, indicating that the non-wetting phase (which is assumed to be lighter than the wetting phase) preferentially rises towards the cap rock. The larger the effects of surface tension (i.e. small Bo) the more the capillary pressure acts to spread out the distribution of non-wetting phase.

2.5 Consolidation

Consolidation refers to the ability of a granular porous medium such as a soil to compact under its own weight, or by the imposition of an overburden pressure. The grains of the medium rearrange themselves under the pressure, thus reducing the porosity and in the process pore fluid is expelled. Since the porosity is no longer constant, we have to postulate a relation between the porosity ϕ and the pore pressure p. In practice, it is found that soils, when compressed, obey a (non-reversible) relation between ϕ and the *effective pressure*

$$p_{\mathrm{eff}} = P - p, \tag{2.195}$$

where P is the overburden pressure.

The concept of effective pressure, or more generally effective stress, is an extremely important one. The idea is that the total imposed pressure (e. g., the overburden pressure due to the weight of the rock or soil) is borne by both the pore fluid and the porous medium. The pore fluid is typically at a lower pressure than the overburden, and the extra stress (the effective stress) is that which is applied through grain to grain contacts. Thus the effective pressure is that which is transmitted through the porous medium, and it is in consequence of this that the medium responds to the effective stress; in particular, the characteristic relation between ϕ and p_{eff} represents the nonlinear pseudo-elastic effect of compression.

The dependence of the effective pressure on porosity is non-trivial and involves hysteresis, as indicated in figure 2.19. Specifically, a soil follows the *normal consolidation line* providing consolidation is occurring, i.e $\dot{p}_{\mathrm{eff}} > 0$. However, if at some point the effective pressure is reduced, only a partial recovery of ϕ takes place. When p_{eff} is increased again, ϕ more or less retraces its (overconsolidated) path to the normal consolidation line, and then resumes its normal consolidation path. Here we will ignore effects of hysteresis, as in (3.147).

When modelling groundwater flow in a consolidating medium, we must take account also of deformation of the medium itself. In turn, this requires prescription of a constitutive rheology for the deformable matrix. This is often a complex matter, but luckily in one dimension, the issue does not arise, and a one-dimensional model is often what is of practical interest. We take z to point vertically upwards, and let v and w be the linear (or *phase-averaged*) velocities of liquid and solid, respectively. Then ϕv and $(1-\phi)w$ are the respective fluxes, and conservation of mass of each phase requires

$$\begin{aligned} \frac{\partial \phi}{\partial t} + \frac{\partial (\phi v)}{\partial z} &= 0, \\ -\frac{\partial \phi}{\partial t} + \frac{\partial}{\partial z}\{(1-\phi)w\} &= 0; \end{aligned} \tag{2.196}$$

Darcy's law is then

$$\phi(v-w) = -\frac{k}{\mu}\left[\frac{\partial p}{\partial z} + \rho_l g\right], \tag{2.197}$$

while the overburden pressure satisfies

$$\frac{\partial P}{\partial z} = -[\rho_s(1-\phi) + \rho_l \phi]g, \quad P = P_0 \quad \text{on} \quad z = h; \tag{2.198}$$

here $z = h$ represents the ground surface and P_0 is the applied load. The effective pressure is just $-p_{\text{eff}} = P - p$.

Note that by adding the two mass conservation equations and integrating, we have

$$\phi v + (1-\phi)w = q(t), \tag{2.199}$$

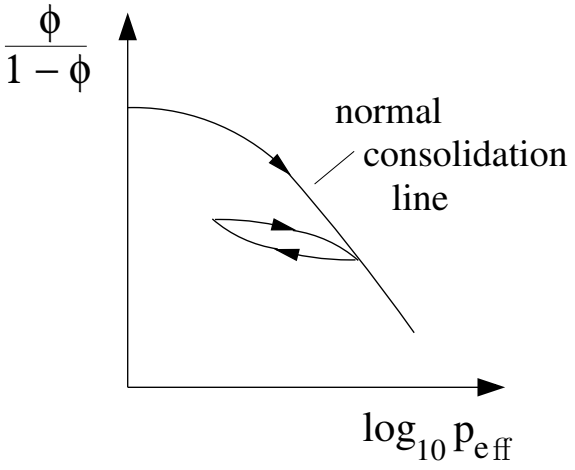

Figure 2.19: Form of the relationship between porosity and effective pressure. A hysteretic decompression-reconsolidation loop is indicated. In soil mechanics this relationship is often written in terms of the *void ratio* $e = \phi/(1-\phi)$, and specifically $e = e_0 - C_c \log_{10} p_{\text{eff}}$, where C_c is the *compression index*.

which can be determined from the boundary conditions. In particular, if we assume an impermeable basement where $v = w = 0$, then $q = 0$ and

$$w = -\frac{\phi v}{1-\phi}, \quad \phi(v-w) = -w. \tag{2.200}$$

We use the definition of the effective pressure in (2.195), together with (2.198) and (2.199), to derive the equation

$$\frac{\partial \phi}{\partial t} = -\frac{\partial}{\partial z}\left[\frac{k}{\mu}(1-\phi)\left\{\frac{\partial p_{\text{eff}}}{\partial z} + \Delta\rho(1-\phi)g\right\}\right], \tag{2.201}$$

where $\Delta\rho = \rho_s - \rho_l$, and since $p_{\text{eff}}(\phi)$ is a monotonically decreasing function, this brings us back to the Richards equation (2.125). Specifically, we can write (2.201) in the form

$$\phi_t + V_z = \left[D\phi_z\right]_z, \tag{2.202}$$

where

$$V(\phi) = \frac{k(\phi)\Delta\rho g}{\mu}(1-\phi)^2, \quad D = -\frac{k(\phi)}{\mu}(1-\phi)p'_{\text{eff}}(\phi), \tag{2.203}$$

and this can be compared to (2.125).

A commonly used expression in soil mechanics for the relationship between effective pressure and porosity is a logarithmic dependence of the *void ratio* $\phi/(1-\phi)$ on p_{eff}, as mentioned in figure 2.19. The *normal consolidation line* for a soil is that part of the yield surface on which the shear stress vanishes, and we may take

$$\frac{\phi}{1-\phi} = e_0 - C_c \log_{10}\left(\frac{p_{\text{eff}}}{p^0_{\text{eff}}}\right); \tag{2.204}$$

the quantity C_c is called the *compression index*. Note that this prescription will not be valid at small effective pressure, since as $p_{\text{eff}} \to 0$, the porosity will tend to its value at loose packing, which we denote as ϕ_0. This gives p_{eff} as a monotonically decreasing function of ϕ for $0 < \phi < 1$, and in particular,

$$p'_{\text{eff}}(\phi) = -\frac{0.43\, p_{\text{eff}}}{C_c(1-\phi)^2}, \tag{2.205}$$

where $0.43 \approx \ln 10$. In this case,

$$D = \frac{0.43\, k(\phi) p_{\text{eff}}}{\mu C_c(1-\phi)}. \tag{2.206}$$

The diffusion coefficient D is sometimes written as c_v, and is known as the *coefficient of consolidation*. If we use values $\mu = 10^{-3}$ Pa s, $p_{\text{eff}} = 10^4$ Pa, $k = 10^{-14}$ m^2 (for silt), $C_c = 0.1$ and $\phi = 0.4$, then $D \sim 10^{-6}$ m^2 s^{-1}. Of course this value depends strongly on the permeability, or equivalently the hydraulic conductivity $K = \dfrac{k\rho g}{\mu}$. For the silt permeability, $K \sim 3$ m y^{-1}, whereas actual soils (with organic matter, worm burrows,

etc.), typically have hydraulic conductivities ~ 1 m d^{-1}, which is about a hundred times larger, and would give a corresponding diffusion coefficient of $D \sim 10^{-4}$ m^2 s^{-1}.

We suppose these equations apply in a vertical column $0 < z < h$, for which suitable boundary conditions are (with an impermeable basement and no surface load)

$$\begin{aligned} v = w = 0 \quad &\text{at} \quad z = 0, \\ \phi = \phi_0,\ \dot{h} = w \quad &\text{at} \quad z = h, \end{aligned} \tag{2.207}$$

and with an initial condition for ϕ. Note that by comparing $(2.196)_1$ and (2.202), and using (2.200),

$$w = -\frac{(V - D\phi_z)}{1 - \phi}. \tag{2.208}$$

Therefore the boundary conditions in (2.207) collapse to

$$\begin{aligned} V - D\phi_z = 0 \quad &\text{at} \quad z = 0, \\ \phi = \phi_0,\ \dot{h} = -\frac{(V - D\phi_z)}{1 - \phi} \quad &\text{at} \quad z = h. \end{aligned} \tag{2.209}$$

In the steady state, it follows that $V - D\phi_z = 0$, and thus

$$\int_{\phi}^{\phi_0} \frac{D(\phi)\, d\phi}{V(\phi)} = h - z. \tag{2.210}$$

If C_c is small (and typical values are in the range $C_c \leq 0.1$) then ϕ varies little, and we can suppose V and D are approximately constant. In this case, the consolidation equation takes the simpler form

$$\phi_t = D\phi_{zz}, \tag{2.211}$$

together with (2.209), and the steady solution (2.210) is just

$$\phi = \phi_0 - \frac{V}{D}(h_0 - z). \tag{2.212}$$

We now consider settlement of the ground after imposition of a surface load pressure ΔP. We suppose the final steady state has depth h_∞, so that the final steady solution (with D and V being constant) is

$$\phi^* = \phi_\infty - \frac{V}{D}(h_\infty - z), \tag{2.213}$$

and $\phi_\infty = \phi(p_{\text{eff}}^\infty)$, where p_{eff}^∞ is the applied surface effective pressure. With no initial surface load, $p_{\text{eff}}^\infty = \Delta P$, the prescribed surface load, and so (for small changes in ϕ)

$$\phi_\infty \approx \phi_0 - |\phi'(0)|\Delta P. \tag{2.214}$$

We perturb the system by writing

$$\phi = \phi^*(z) + \Phi, \quad h = h_\infty + \eta, \tag{2.215}$$

and then linearising the equation and boundary conditions. This leads to

$$\begin{aligned} \Phi_t &= D\Phi_{zz}, \\ \Phi_z = 0 &\quad \text{on} \quad z = 0, \\ \frac{V}{D}\eta + \Phi = 0, &\qquad \eta_t = \frac{D\Phi_z}{1-\phi_\infty} \quad \text{on} \quad z = h_\infty. \end{aligned} \tag{2.216}$$

Eliminating η from the surface boundary condition gives

$$\Phi_t + \frac{V\Phi_z}{1-\phi_\infty} = 0 \quad \text{on} \quad z = h_\infty. \tag{2.217}$$

Subtracting the initial condition from the final condition, we find

$$\Phi = \phi_0 - \phi_\infty - \frac{V}{D}(h_0 - h_\infty), \quad \eta = h_0 - h_\infty \quad \text{at} \quad t = 0. \tag{2.218}$$

At this point we realise that the initial depth h is unconstrained. It is in fact determined by the volume of solids in the domain (which, unlike the volume of water which is squeezed out the top, is conserved). Thus we require

$$\int_0^{h_\infty+\eta} [1 - (\phi^* + \Phi)]\, dz = \int_0^{h_\infty} (1 - \phi^*)\, dz, \tag{2.219}$$

and linearising this leads to the normalising condition

$$\int_0^{h_\infty} \Phi\, dz = (1 - \phi_\infty)\eta. \tag{2.220}$$

This is consistent with (2.216) (as it must be), and it provides the necessary relation between h_0 and h_∞, which is, using (2.214),

$$\frac{h_0 - h_\infty}{h_\infty} = \frac{|\phi'(0)|\Delta P}{1 - \phi_\infty + \dfrac{Vh_\infty}{D}}, \tag{2.221}$$

and this is the (relative) settlement due to a given load.

The other quantity of interest is the settlement time. The normal mode solutions of (2.216) are

$$\Phi = e^{-Ds^2t} \cos sz, \tag{2.222}$$

where

$$\tan\kappa = -\frac{\kappa}{Pe}, \quad \kappa = sh_\infty, \quad Pe = \frac{h_\infty V}{D(1-\phi_\infty)}; \tag{2.223}$$

here Pe is a suitable Péclet number for the flow, and s is the wavenumber (normally one uses k, but that is already taken for the permeability). It is graphically straightforward to see that there is an infinite number of values of $\kappa_1, \kappa_2, \ldots$ (positive, without loss of generality) satisfying (2.223), with $(n - \frac{1}{2})\pi < \kappa_n < n\pi$. The settlement or consolidation time scale t_c is essentially determined by κ_1, and is thus

$$t_c \sim \frac{h_\infty^2}{D\kappa_1^2}, \tag{2.224}$$

where κ_1 lies between $\frac{1}{2}\pi$ and π. It depends primarily on the permeability k. If we use (2.206), and take $k \sim 10^{-14}$ m^2 (silt), $C_c = 0.1$, $\phi = 0.3$, $\mu = 10^{-3}$ Pa s, $P_0 = 10^5$ Pa (a small house), then $D \sim 0.6 \times 10^{-5}$ m^2 s^{-1}. Similarly, with $\Delta\rho = 2 \times 10^3$ kg m^{-3}, we find $V \sim 10^{-7}$ m s^{-1}, and so, if we take $h_\infty = 10$ m, the Péclet number is $Pe \sim 0.23$; not extremely small, but small enough to use the approximation of small Pe in (2.223). When Pe is small, $\kappa \approx \frac{1}{2}\pi$, and so 14.82

$$t_c \sim \frac{4h_\infty^2}{\pi^2 D}, \tag{2.225}$$

which gives $t_c \sim 3$ months.

Exercises

2.1 Show that for a porous medium idealised as a cubical network of tubes, the permeability is given (approximately) by $k = d_p^2\phi^2/72\pi$, where d_p is the grain size. How is the result modified if the pore space is taken to consist of planar sheets between identical cubical blocks? (The volume flux per unit width between two parallel plates a distance h apart is $-h^3p'/12\mu$, where p' is the pressure gradient.)

2.2 Groundwater flows between an impermeable basement at $z = h_b(x, y, t)$ and a phreatic surface at $z = z_p(x, y, t)$. Write down the equations governing the flow, and by using the Dupuit approximation, show that the saturated depth h satisfies

$$\phi h_t = \frac{k\rho g}{\mu}\boldsymbol{\nabla}.[h\boldsymbol{\nabla}z_p],$$

where $\boldsymbol{\nabla} = (\partial/\partial x, \partial/\partial y)$. Deduce that a suitable time scale for flows in an aquifer of typical depth h_0 and extent l is $t_{gw} = \phi\mu l^2/k\rho g h_0$.

I live a kilometer from the river, on top of a layer of sediments 100 m thick (below which is impermeable basement). What sort of sediments would those need to be if the river responds to rainfall at my house within a day; within a year?

2.3 A two-dimensional earth dam with vertical sides at $x = 0$ and $x = l$ has a reservoir on one side ($x < 0$) where the water depth is h_0, and horizontal dry

land on the other side, in $x > l$. The dam is underlain by an impermeable basement at $z = 0$.

Write down the equations describing the saturated groundwater flow, and show that they can be written in the dimensionless form

$$u = -p_x, \quad \varepsilon^2 w = -(p_z + 1),$$

$$p_{zz} + \varepsilon^2 p_{xx} = 0,$$

and define the parameter ε. Write down suitable boundary conditions on the impermeable basement, and on the phreatic surface $z = h(x, t)$.

Assuming $\varepsilon \ll 1$, derive the Dupuit-Forchheimer approximation for h,

$$h_t = (hh_x)_x \ \text{ in } \ 0 < x < 1.$$

Show that a suitable boundary condition for h at $x = 0$ (the dam end) is

$$h = 1 \quad \text{at} \quad x = 0.$$

Now define the quantity

$$U = \int_0^h p \, dz,$$

and show that the horizontal flux

$$q = \int_0^h u \, dz = -\frac{\partial U}{\partial x}.$$

Hence show that the conditions of hydrostatic pressure at $x = 0$ and constant (atmospheric) pressure at $x = 1$ (the seepage face) imply that

$$\int_0^1 q \, dx = \tfrac{1}{2}.$$

Deduce that, if the Dupuit approximation for the flux is valid all the way to the toe of the dam at $x = 1$, then $h = 0$ at $x = 1$, and show that in the steady state, the (dimensional) discharge at the seepage face is

$$q_D = \frac{k\rho g h_0^2}{2\mu l}.$$

Supposing the above description of the solution away from the toe to be valid, show that a possible boundary layer structure near $x = 1$ can be described by writing

$$x = 1 - \varepsilon^2 X, \quad h = \varepsilon H, \quad z = \varepsilon Z, \quad p = \varepsilon P,$$

and write down the resulting leading order boundary value problem for P.

2.4 I get my water supply from a well in my garden. The well is of depth h_0 (relative to the height of the water table a large distance away) and radius r_0. Show that the Dupuit approximation for the water table height h is

$$\phi\frac{\partial h}{\partial t} = \frac{k\rho g}{\mu}\frac{1}{r}\frac{\partial}{\partial r}\left(rh\frac{\partial h}{\partial r}\right).$$

If my well is supplied from a reservoir at $r = l$, where $h = h_0$, and I withdraw a constant water flux q_0, find a steady solution for h, and deduce that my well will run dry if

$$q_0 > \frac{\pi k\rho g h_0^2}{\mu \ln[l/r_0]}.$$

Use plausible values to estimate the maximum yield (gallons per day) I can use if my well is drilled through sand, silt or clay, respectively.

2.5 A volume V of effluent is released into the ground at a point ($r = 0$) at time t. Use the Dupuit approximation to motivate the model

$$\phi\frac{\partial h}{\partial t} = \frac{k\rho g}{\mu}\frac{1}{r}\frac{\partial}{\partial r}\left(rh\frac{\partial h}{\partial r}\right),$$

$$h = h_0 \ \text{ at } \ t = 0,\ r > 0,$$

$$\int_0^\infty r(h - h_0)dr = V/2\pi,\ t > 0,$$

where h_0 is the initial height of the water table above an impermeable basement. Find suitable similarity solutions in the two cases (i) $h_0 = 0$ (ii) $h_0 > 0$, $h - h_0 \ll h_0$, and comment on the differences you find.

2.6 Rain falls steadily at a rate q (volume per unit area per unit time) on a soil of saturated hydraulic conductivity K_0 ($= k_0\rho_w g/\mu$, where k_0 is the saturated permeability). By plotting the relative permeability k_r and suction characteristic $\sigma\psi/d$ as functions of S (assuming a residual liquid saturation S_0), show that a reasonable form to choose for $k_r(\psi)$ is $k_r = e^{-c\psi}$. If the water table is at depth h, show that, in a steady state, ψ is given as a function of the dimensionless depth $z^* = z/z_c$, where $z_c = \sigma/\rho_w g d$ (σ is the surface tension, d the grain size) by

$$h^* - z^* = \tfrac{1}{2}\psi - \frac{1}{c}\ln\left[\frac{\sinh\{\frac{1}{2}(\ln\frac{1}{q^*} - c\psi)\}}{\sinh\{\frac{1}{2}\ln\frac{1}{q^*}\}}\right],$$

where $h^* = h/z_c$, providing $q^* = q/K_0 < 1$. Deduce that if $h \gg z_c$, then $\psi \approx \frac{1}{c}\ln\frac{1}{q^*}$ near the surface. What happens if $q > K_0$?

2.7 Derive the Richards equation

$$\phi\frac{\partial S}{\partial t} = -\frac{\partial}{\partial z}\left[\frac{k_0}{\mu}k_r(S)\left\{\frac{\partial p_c}{\partial z} + \rho_w g\right\}\right]$$

for one-dimensional infiltration of water into a dry soil, explaining the meaning of the terms, and giving suitable boundary conditions when the surface flux q is prescribed. Show that if the surface flux is large compared with $k_0\rho_w g/\mu$, where k_0 is the saturated permeability, then the Richards equation can be approximated, in suitable non-dimensional form, by a nonlinear diffusion equation of the form

$$\frac{\partial S}{\partial t} = \frac{\partial}{\partial z}\left[D\frac{\partial S}{\partial z}\right].$$

Show that, if $D = S^m$, a similarity solution exists in the form

$$S = t^\alpha F(\eta), \quad \eta = z/t^\beta,$$

where $\alpha = \dfrac{1}{m+2}$, $\beta = \dfrac{m+1}{m+2}$, and F satisfies

$$(F^m F')' = \alpha F - \beta\eta F', \quad F^m F' = -1 \ \text{ at } \ \eta = 0, \quad F \to 0 \ \text{ as } \ \eta \to \infty.$$

Deduce that

$$F^m F' = -(\alpha+\beta)\int_\eta^{\eta_0} F d\eta - \beta\eta F,$$

where η_0 (which may be ∞) is where F first reaches zero. Deduce that $F' < 0$, and hence that η_0 must be finite, and is determined by

$$\int_0^{\eta_0} F\, d\eta = \frac{1}{\alpha+\beta}.$$

What happens for $t > F(0)^{-1/\alpha}$?

2.8 Write down the equations describing one-dimensional consolidation of wet sediments in terms of the variables $\phi, v, w, p, p_{\text{eff}}$, these being the porosity, solid and liquid (linear) velocities, and the pore and effective pressures. Neglect the effect of gravity.

Saturated sediments of depth h lie on a rigid but permeable (to water) basement, through which a water flux W is removed. Show that

$$w = \frac{k}{\mu}\frac{\partial p}{\partial z} - W,$$

and deduce that ϕ satisfies the equation

$$\frac{\partial \phi}{\partial t} = \frac{\partial}{\partial z}\left[(1-\phi)\left\{\frac{k}{\mu}\frac{\partial p}{\partial z} - W\right\}\right].$$

If the sediments are overlain by water, so that $p =$ constant (take $p = 0$) at $z = h$, and if $\phi = \phi_0 + p/K$, where the compressibility K is large (so $\phi \approx \phi_0$), show that a suitable reduction of the model is

$$\frac{\partial p}{\partial t} - W\frac{\partial p}{\partial z} = c\frac{\partial^2 p}{\partial z^2},$$

where $c = K(1-\phi_0)k/\mu$, and $p = 0$ on $z = h$, $p_z = \mu W/k$. Non-dimensionalise the model using the length scale h, time scale h^2/c, and pressure scale $\mu W h/k$. Hence describe the solution if the parameter $\varepsilon = \mu W h/k$ is small, and find the rate of surface subsidence. What has this to do with Venice?

2.9 Write down a model for vertical flow of two immiscible fluids in a porous medium. Deduce that the saturation S of the wetting phase satisfies the equation

$$\phi\frac{\partial S}{\partial t} + \frac{\partial}{\partial z}\left[M_{\text{eff}}\left\{\frac{q}{M_{nw}} + g\Delta\rho\right\}\right] = -\frac{\partial}{\partial z}\left[M_{\text{eff}}\frac{\partial p_c}{\partial z}\right],$$

where z is a coordinate pointing *downwards*,

$$p_c = p_{nw} - p_w, \quad \Delta\rho = \rho_w - \rho_{nw}, \quad M_{\text{eff}}^{-1} = (M_w^{-1} + M_{nw}^{-1}),$$

q is the total downward flux, and the suffixes w and nw refer to the wetting and non-wetting fluid respectively. Define the phase mobilities M_i. Give a criterion on the capillary suction p_c which allows the Buckley-Leverett approximation to be made, and show that for $q = 0$ and $\mu_w \gg \mu_{nw}$, waves typically propagate downwards and form shocks. What happens if $q \neq 0$? Is the Buckley-Leverett approximation realistic — e.g. for air and water in soil? (Assume $p_c \sim 2\gamma/r_p$, where $\gamma = 70$ mN m^{-1}, and r_p is the pore radius: for clay, silt and sand, take $r_p = 1\ \mu$, $10\ \mu$, $100\ \mu$, respectively.)

2.10 A model for snow melt run-off is given by the following equations:

$$u = \frac{k}{\mu}\left[\frac{\partial p_c}{\partial z} + \rho_l g\right],$$

$$k = k_0 S^3,$$

$$\phi\frac{\partial S}{\partial t} + \frac{\partial u}{\partial z} = 0,$$

$$p_c = p_0\left(\frac{1}{S} - S\right).$$

Explain the meaning of the terms in these equations, and describe the assumptions of the model.

The intrinsic permeability k_0 is given by

$$k_0 = 0.077\ d^2 \exp[-7.8\ \rho_s/\rho_l],$$

where ρ_s and ρ_l are snow and water densities, and d is grain size. Take $d = 1$ mm, $\rho_s = 300$ kg m^{-3}, $\rho_l = 10^3$ kg m^{-3}, $p_0 = 1$ kPa, $\phi = 0.4$, $\mu = 1.8 \times 10^{-3}$ Pa s, $g = 10$ m s^{-2}, and derive a non-dimensional model for melting of a one metre thick snow pack at a rate (i.e. u at the top surface $z = 0$) of 10^{-6} m s^{-1}. Determine whether capillary effects are small; describe the nature of the model equation, and find an approximate solution for the melting of an initially dry snowpack. What is the (meltwater flux) run-off curve?

2.11 Consider the following model, which represents the release of a unit quantity of groundwater at $t = 0$ in an aquifer $-\infty < x < \infty$, when the Dupuit approximation is used:

$$h_t = (hh_x)_x,$$

$$h = 0 \text{ at } t = 0,\ x \neq 0,$$

$$\int_{-\infty}^{\infty} h\,dx = 1$$

(i. e., $h = \delta(x)$ at $t = 0$). Show that a similarity solution to this problem exists in the form

$$h = t^{-1/3} g(\xi), \quad \xi = x/t^{1/3},$$

and find the equation and boundary conditions satisfied by g. Show that the water body spreads at a finite rate, and calculate what this is.

Formulate the equivalent problem in three dimensions, and write down the equation satisfied by the similarity form of the solution, assuming cylindrical symmetry. Does this solution have the same properties as the one-dimensional solution?

Chapter 3

Convection

Convection is the fluid motion induced by buoyancy; buoyancy is the property of a fluid whereby its density depends on external properties. The most common form of convection is *thermal convection*, which occurs due to the dependence of density on temperature: warm fluid is light, and therefore rises. Everyday examples of this are the circulation induced by a convector heater, or the motion which can be seen in a saucepan of oil when it is heated. (In the latter case, one can see convection rolls in the fluid, regular but time-dependent.) Another common form of convection is *compositional convection*, which is induced by density changes dependent on composition. An example of this occurs during the formation of sea ice in the polar regions. As salty sea water freezes, it rejects the salt (the ice is almost pure water substance), and the resulting salty water is denser than the sea water from which it forms, and thus induces a convective motion below the ice. Below, we discuss three geophysical examples from convection, but convection is everywhere: it drives the oceanic circulation, it drives the atmospheric circulation, it causes thunderstorms, it occurs in glass manufacture, in a settling pint of Guinness, in back boilers, in solar panels. And, it has formed the thematic core of the subject of geophysical fluid dynamics for almost a century.

3.1 Mantle convection

Most people have heard of continental drift, the process whereby the Earth's continents drift apart relative to each other. The Atlantic Ocean is widening at the rate of several centimetres a year, the crashing of India into Asia over the last 50 My (fifty million years) has caused the continuing uplift of the Himalayas, Scotland used to be joined to Newfoundland. The continents ride, like rafts of debris, on the tectonic plates of the Earth, which separate at mid-ocean ridges and converge at subduction zones. The theory of plate tectonics, which originated with the work of Wegener and Holmes in the early part of the twentieth century, and which was finally accepted by geophysicists in the 'plate tectonics revolution' of the 1960's, describes the surface of the Earth as being split up into some thirteen major tectonic plates: see figure

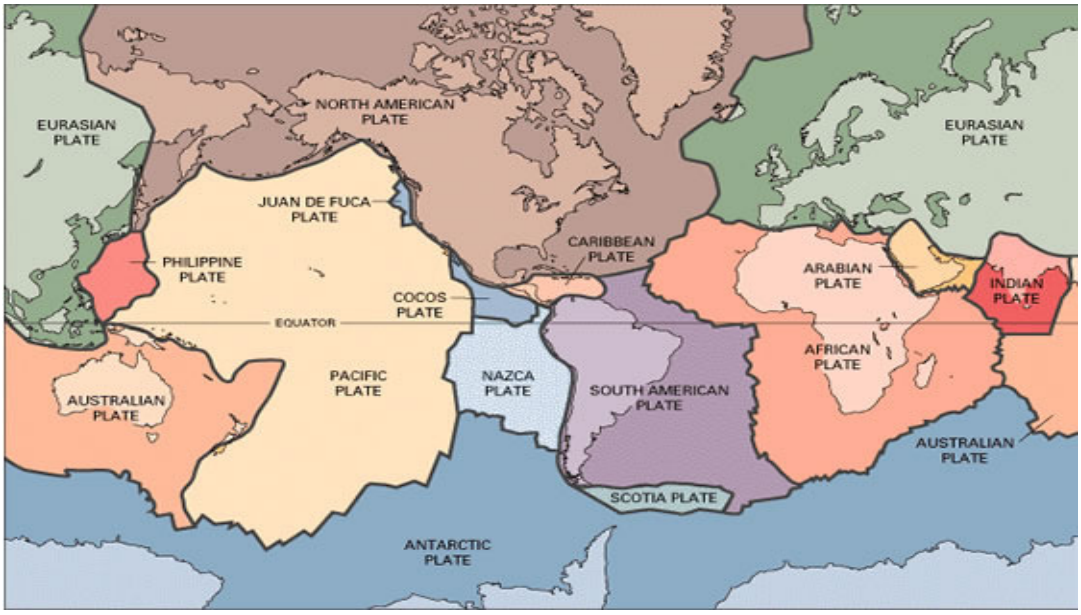

Figure 3.1: The tectonic plates of the Earth.

3.1. These plates move relative to each other across the surface, and this motion is the surface manifestation of a convective motion in the Earth's *mantle*, which is the part of the Earth from the surface to a depth of about 3,000 kilometres, and which consists of an assemblage of polycrystalline silicate rocks. Upwelling occurs at mid-ocean ridges, for example the mid-Atlantic ridge which passes through Iceland, and the East Pacific Rise off the coast of South America, which passes through the Galapagos Islands. The plates sink into the mantle at subduction zones, which adjoin continental boundaries, and which are associated with the presence of oceanic trenches.

The plates are so called because they are conceived of as moving quasi-rigidly. They are in fact the cold upper thermal boundary layers of the convective motion, in-

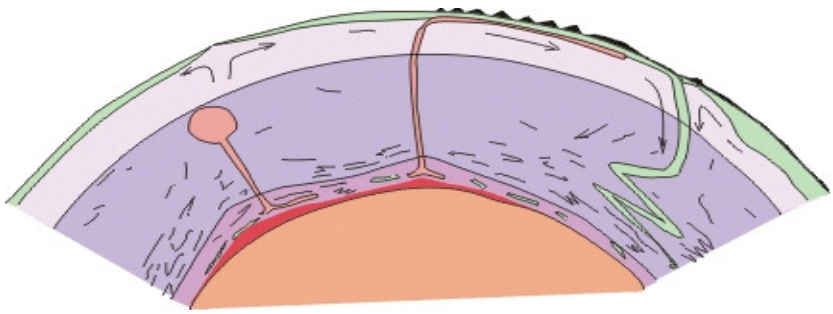

Figure 3.2: A cartoon of mantle convection. We see plumes, mid-ocean ridges, subducting slabs.

dicated schematically in figure 3.2, and are plate-like because the strong temperature dependence of mantle viscosity renders these relatively cold rocks extremely viscous. One may wonder how the mantle moves at all, consisting as it does of mostly solid polycrystalline rocks. In fact, solids will deform just as fluids do when subjected to stress. The deformation is enabled by the migration of dislocations within the crystalline lattice of the solid grains of the rock. The effective viscosity of the Earth's mantle is a whopping 10^{21} Pa s; this is about eight orders of magnituse greater than the viscosity of ice, and twenty-four orders greater than the viscosity of water.

The reason that the mantle convects is that the Earth is cooling. The primordial heat of formation has gradually been lost over the Earth's history, but the central core of the planet is still very hot; some six thousand degrees Celsius at the centre of the Earth. This heat from the core is instrumental in heating the mantle from below, and driving the convective flow. Radioactive heating also contributes to an extent which is not certain, but which is thought to be significant.

3.2 The Earth's core

Part of the heat which drives mantle convection is derived from cooling the Earth's core. The core is the part of the Earth which lies between its centre and the mantle. Like the mantle, it is also some three thousand kilometres deep, and consists of a molten outer core of iron, alloyed with some lighter element, usually thought to be sulphur or oxygen, in a concentration of some 10%. The inner core is solid (pure) iron, of radius 1,000 km. It is generally thought that the core was initially molten throughout, and that the inner core has gradually solidified from the outer core over the course of geological time. It is the consequent release of latent heat which, at least partly, powers mantle convection.

One may wonder how the outer core can be liquid, and the inner core solid, if the inner core is hotter (as it must be). The reason for this is that the solidification temperature (actually the liquidus temperature, see below) depends on pressure, through the Clapeyron effect. This is the effect whereby a pressure cooker works: the boiling temperature increases with pressure, and similarly, the solidification temperature of the outer core iron alloy increases with pressure, and thus also depth. Thus, the inner core can be below the solidification temperature because of the greater pressure there.

The convection in the outer core is partly due to the dependence of density on temperature, but the primary dependence is, as often the case when composition varies, due to the dependence of density on the concentration of sulphur (or oxygen). In order to understand how the solidification of the inner core leads to convection, we need to understand the general thermodynamic way in which melting and solidification occur in multi-component materials. This is illustrated in figure 3.3, which indicates how the solidification temperatures vary with composition in a two-component melt. At a given temperature, there are two curves which describe the concentrations of the solid and liquid, when these are in thermodynamic equilibrium with each other. These two curves are called the solidus and liquidus, respectively. Often there are two sets of

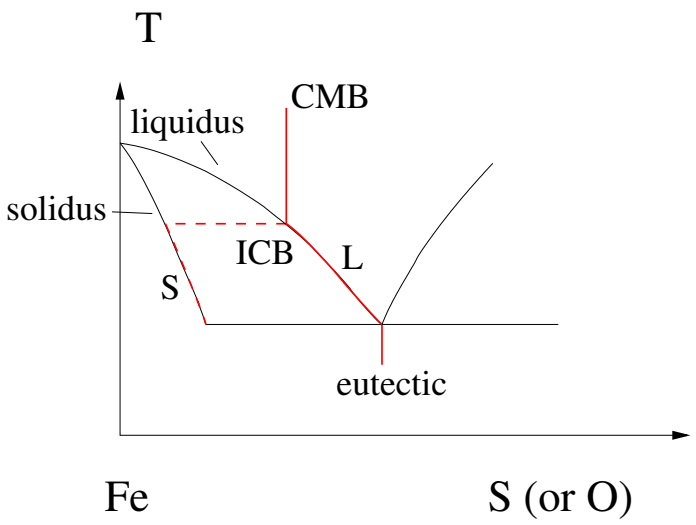

Figure 3.3: Typical phase diagram for a two-component alloy with a eutectic point. When the liquid reaches the liquidus (L), the resulting solid has the concentration of the solidus (S). When the liquid reaches the eutectic point, two solids, iron-rich and sulphur-rich respectively, will be formed.

solidus and liquidus curves, and they meet at a point called the eutectic point. The way in which a liquid alloy solidifies is then indicated by the red line in figure 3.3. In the outer core, the composition is relatively constant, but the temperature decreases (relative to the liquidus) from the core-mantle boundary (CMB) to the inner core boundary (ICB), where solidification occurs. (The phase diagram is indicated as if at constant pressure; in reality, the curves will also vary with pressure.)

At this temperature, the solid which crystallises has the solidus concentration, which is richer in iron than the liquid, and so as the temperature cools during freezing, the liquid concentration of sulphur or oxygen increases because of its rejection at the freezing interface. It is this source of buoyancy which provides the driving force for compositional convection.

Actually, it is typically the case that when alloys solidify, they do not form a solid with a clear interface. Rather, such a situation is typically *morphologically unstable*, and a dendritic mush consisting of a solid–liquid mixture is formed, as shown in figure 3.4. The convection caused by the release of light fluid now occurs throughout the mush, and leads to the formation of narrow 'chimneys', from which plumes emerge.

In the Earth's core, it is this convection which forms the magnetic field. Convection in an electrically conducting fluid causes a magnetic field to grow, providing the magnetic diffusivity is sufficiently small, through the action of the Lorentz force. The study of such instabilities is a central part of the subject of magnetohydrodynamics.

Figure 3.4: A dendritic mush in the solidification of ammonium chloride in the laboratory. Convection occurs within the mush, leading to the formation of 'chimneys' which act as sources of plumes in the residual melt. Photo courtesy of Grae Worster.

3.3 Magma chambers

Our final example of convection arises in the formation and cooling of magma chambers. When mantle rock upwells, either at mid-ocean ridges, or in isolated thermal plumes such as that below Hawaii, the slight excess temperature causes the rock to partially melt. It is thought that the melt fraction can then ascend through the residual porous matrix, forming rivulets and channels which allow the escape of the magma through the lithosphere to the crust.[1] As the magma ascends into the crust, it can typically encounter unconformities, where the rock types alter, and where the density may be less than that of the magma. In that case, the magma will stop rising, but will spread laterally, simultaneously uplifting the overlying strata. Thus forms the *laccolith*, a magmatic intrusion, and over the course of time such intrusions, or magma chambers, will solidify, forming huge cauldrons of rock which may later be exposed at the Earth's surface.

Convection undoubtedly occurs in such chambers, which may be tens of kilometres in extent. The hot magma is continuously chilled at the roof and sides of the chamber, and this leads to convective currents continually draining towards the floor of the chamber. There they will accumulate, leading to a cold, crystal-rich layer ly-

[1]The *lithosphere* is the cold surface boundary layer of the convecting mantle, of depth some 100 km in the oceanic mantle, somewhat greater beneath continents; the crust is a relatively thin layer of rocks near the surface, formed through partial melting of the mantle and the resulting volcanism.

Figure 3.5: Graded layering in the Skaergaard intrusion. Photograph courtesy of Kurt Hollocher.

ing stagnant below the convecting upper portion. This is essentially the filling box mechanism which is discussed further below.

Magmas are multi-component alloys, and their convective solidification can lead to various exotic phenomena. The phase diagram of the type in figure 3.3 causes chemical differentiation on the large scale (in metal alloy castings this is called macrosegregation). For example, in an olivine–plagioclase magma, the heavy olivine will crystallise out first, and the crystals may settle to the base of the chamber. The residual liquid is then plagioclase-rich and lighter. So the end result would be a chamber having two distinct layers. Successive injections of magma may then lead to a sequence of such layers, as is seen in the Scottish island of Rum, and this has been suggested as an explanation for these particular layers.

Other magma chambers show layering at a much finer scale, and the origin of these layers is a mystery. An example is shown in figure 3.5. The layers are reminiscent of double-diffusive layering, which we discuss in section 3.6.2, but efforts to build a theory round this idea, or indeed any other, have so far not met with success.

3.4 Rayleigh–Bénard convection

The simplest model of convection is the classical Rayleigh-Bénard model in which a layer of fluid is heated from below, by application of a prescribed temperature

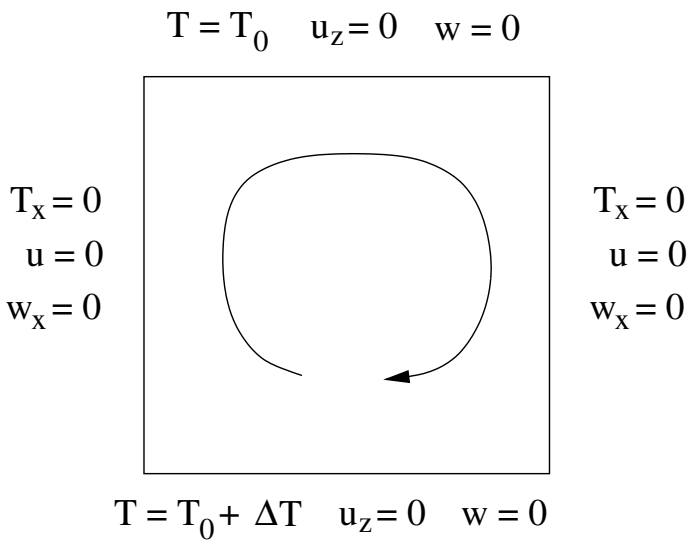

Figure 3.6: Geometry of a convection cell.

difference across the layer. Depending on the nature of the boundaries, one may have a no slip condition or a no shear stress condition applied at the bounding surfaces. For the case of mantle convection, one conceives of both the oceans (or atmosphere) and the underlying fluid outer core as exerting no stress on the extremely viscous mantle, so that no stress conditions are appropriate, and in fact it turns out that this is the simplest case to consider. The geometry of the flow we consider is shown in figure 3.6. It is convenient to assume lateral boundaries, although in a wide layer, these simply represent the convection cell walls, and can be an arbitrary distance apart.

The equations describing the flow are the Navier-Stokes equations, allied with the energy equation and an equation of state, and can be written in the form

$$\begin{aligned} \rho_t + \boldsymbol{\nabla}.(\rho\mathbf{u}) &= 0, \\ \rho[\mathbf{u}_t + (\mathbf{u}.\boldsymbol{\nabla})\mathbf{u}] &= -\boldsymbol{\nabla}p - \rho g\mathbf{k} + \mu\nabla^2\mathbf{u}, \\ \rho c_p[T_t + \mathbf{u}.\boldsymbol{\nabla}T] &= k\nabla^2 T, \\ \rho &= \rho_0[1-\alpha(T-T_0)]; \end{aligned} \tag{3.1}$$

in these equations, ρ is the density, $\mathbf{u}$ is the velocity, p is the pressure, g is the acceleration due to gravity, $\mathbf{k}$ is the unit upwards vector, μ is viscosity, c_p is the specific heat, T is temperature, k is thermal conductivity, ρ_0 is the density at the reference temperature T_0 at the surface of the fluid layer, and α is the thermal expansion coefficient. The boundary conditions for the flow are indicated in figure 3.6, and correspond to prescribed temperature at top and bottom, no flow through the boundaries, and no shear stress at the boundaries. The lateral boundaries represent stress free 'walls', but as mentioned above, these simply indicate the boundaries of the convection cells

(across which there is no heat transport, hence the no flux condition for temperature).

To proceed, we non-dimensionalise the variables as follows. We use the convective time scale, and a thermally related velocity scale, and use the depth of the box d as the length scale:

$$\begin{aligned} \mathbf{u} \sim \frac{\kappa}{d}, \quad \kappa = \frac{k}{\rho_0 c_p}, \qquad t \sim \frac{d^2}{\kappa}, \quad \mathbf{x} \sim d, \\ p - [p_0 + \rho_0 g(d-z)] \sim \frac{\mu\kappa}{d^2}, \qquad T - T_0 \sim \Delta T. \end{aligned} \tag{3.2}$$

Here p_0 is the (prescribed) pressure at the surface, which we take as constant. We would also scale $\rho \sim \rho_0$, but in the scaled equations below, the density has been algebraically eliminated. The scaled equations take the form

$$\begin{aligned} -BT_t + \boldsymbol{\nabla}.[(1-BT)\mathbf{u}] &= 0, \\ \frac{1}{Pr}[1-BT][\mathbf{u}_t + (\mathbf{u}.\boldsymbol{\nabla})\mathbf{u}] &= -\boldsymbol{\nabla}p + Ra\,T\mathbf{k} + \nabla^2\mathbf{u}, \\ (1-BT)(T_t + \mathbf{u}.\boldsymbol{\nabla}T) &= \nabla^2 T, \end{aligned} \tag{3.3}$$

and the dimensionless parameters are defined as

$$B = \alpha\Delta T, \quad Pr = \frac{\mu}{\rho_0\kappa}, \quad Ra = \frac{\alpha\rho_0\Delta T g d^3}{\mu\kappa}; \tag{3.4}$$

the parameters Ra and Pr are known as the Rayleigh and Prandtl numbers, respectively. The Prandtl number is a property of the fluid; for air it is 0.7, and for water it is 7. The Rayleigh number is a measure of the strength of the heating. As we shall see, convective motion occurs if the Rayleigh number is large enough, and it becomes vigorous if the Rayleigh number is large. The parameter B might be termed a Boussinesq number, although this is not common usage.

Suppose we think of values typical for a layer of water in a saucepan. We take $d = 0.1$ m, $\mu = 2 \times 10^{-3}$ Pa s, $\Delta T = 100$ K, $\alpha = 3 \times 10^{-5}$ K^{-1}, $\rho_0 = 10^3$ kg m^{-3}, $\kappa = 0.3 \times 10^{-6}$ m^2 s^{-1}, $g = 9.8$ m s^{-2}. Then we have $Pr \approx 7$, $B \approx 3 \times 10^{-3}$, and $Ra \approx 5 \times 10^7$. In this case, we have that $B \ll 1$ and $Ra \gg 1$. This is typically the case. We now make the Boussinesq approximation, which says that $B \ll 1$, and we ignore the terms in B in (3.3). In words, we assume that the density is constant, except in the buoyancy term. The mathematical reason for this exception is that, although $Ra \propto B$ (and so $Ra \to 0$ as $B \to 0$), the actual numerical sizes of the two parameters are typically very different. The adoption of the Boussinesq approximation leads to what are called the Boussinesq equations of thermal convection:

$$\begin{aligned} \boldsymbol{\nabla}.\mathbf{u} &= 0, \\ \frac{1}{Pr}[\mathbf{u}_t + (\mathbf{u}.\boldsymbol{\nabla})\mathbf{u}] &= -\boldsymbol{\nabla}p + \nabla^2\mathbf{u} + Ra\,T\hat{\mathbf{k}}, \\ T_t + \mathbf{u}.\boldsymbol{\nabla}T &= \nabla^2 T, \end{aligned} \tag{3.5}$$

with associated boundary conditions for free slip:

$$\begin{aligned} T = 1, \quad \mathbf{u}.\mathbf{n} = \tau_{nt} = 0 \quad \text{on} \quad z = 0, \\ T = 0, \quad \mathbf{u}.\mathbf{n} = \tau_{nt} = 0 \quad \text{on} \quad z = 1, \end{aligned} \tag{3.6}$$

where τ_{nt} represents the shear stress.

3.4.1 Linear stability

It is convenient to study the problem of the onset of convection in two dimensions (x, z). In this case we can define a stream function ψ which satisfies

$$u = -\psi_z, \quad w = \psi_x. \tag{3.7}$$

(The sign is opposite to the usual convention; for $\psi > 0$ this describes a clockwise circulation.) We eliminate the pressure by taking the curl of the momentum equation $(3.5)_2$, which leads, after some algebra (see also question 3.2), to the pair of equations for ψ and T:

$$\begin{aligned} \frac{1}{Pr}\left[\nabla^2\psi_t + \psi_x\nabla^2\psi_z - \psi_z\nabla^2\psi_x\right] &= Ra\, T_x + \nabla^4\psi, \\ T_t + \psi_x T_z - \psi_z T_x &= \nabla^2 T, \end{aligned} \tag{3.8}$$

with the associated boundary conditions

$$\begin{aligned} \psi = \nabla^2\psi = 0 \quad \text{at} \quad z = 0, 1, \\ T = 0 \quad \text{at} \quad z = 1, \\ T = 1 \quad \text{at} \quad z = 0. \end{aligned} \tag{3.9}$$

In the absence of motion, $\mathbf{u} = \mathbf{0}$, the steady state temperature profile is linear,

$$T = 1 - z, \tag{3.10}$$

and the lithostatic pressure is modified by the addition of

$$p = -\frac{Ra}{2}(1 - z)^2. \tag{3.11}$$

(Even if Ra is large, this represents a small correction to the lithostatic pressure, of relative size $O(B)$.) The stream function is just

$$\psi = 0. \tag{3.12}$$

We define the temperature perturbation θ by

$$T = 1 - z + \theta. \tag{3.13}$$

This yields

$$\begin{aligned} \frac{1}{Pr}\left[\nabla^2\psi_t + \psi_x\nabla^2\psi_z - \psi_z\nabla^2\psi_x\right] &= \nabla^4\psi + Ra\,\theta_x, \\ \theta_t - \psi_x + \psi_x\theta_z - \psi_z\theta_x &= \nabla^2\theta, \end{aligned} \tag{3.14}$$

and the boundary conditions are

$$\psi_{zz} = \psi = \theta = 0 \quad \text{on} \quad z = 0, 1. \tag{3.15}$$

In the Earth's mantle, the Prandtl number is large, and we will now simplify the algebra by putting $Pr = \infty$. This assumption does not in fact affect the result which is obtained for the critical Rayleigh number at the onset of convection. The linear stability of the basic state is determined by neglecting the nonlinear advective terms in the heat equation. We then seek normal modes of wave number k in the form

$$\begin{aligned} \psi &= f(z)e^{\sigma t + ikx}, \\ \theta &= g(z)e^{\sigma t + ikx}, \end{aligned} \tag{3.16}$$

whence f and g satisfy (putting $Pr = \infty$)

$$\begin{aligned} (D^2 - k^2)^2 f + ikRa\,g &= 0, \\ \sigma g - ikf &= (D^2 - k^2)g, \end{aligned} \tag{3.17}$$

where $D = d/dz$, and

$$f = f'' = g = 0 \quad \text{on} \quad z = 0, 1. \tag{3.18}$$

By inspection, solutions are

$$f = \sin m\pi z, \quad g = b\sin m\pi z, \tag{3.19}$$

$(n = 1, 2, ...)$ providing

$$\sigma = \frac{k^2 Ra}{(m^2\pi^2 + k^2)^2} - (m^2\pi^2 + k^2), \tag{3.20}$$

which determines the growth rate for the m-th mode of wave number k.

Since σ is real, instability is characterised by a positive value of σ. We can see that σ decreases as m increases; therefore the value $m = 1$ gives the most unstable value of σ. Also, σ is negative for $k \to 0$ or $k \to \infty$, and has a single maximum. Since σ increases with Ra, we see that $\sigma > 0$ (for $m = 1$) if $Ra > Ra_{ck}$, where

$$Ra_{ck} = \frac{(\pi^2 + k^2)^3}{k^2}. \tag{3.21}$$

In turn, this value of the Rayleigh number depends on the selected wave number k. Since an arbitrary disturbance will excite all wave numbers, it is the minimum

value of Ra_{ck} which determines the absolute threshold for stability. The minimum is obtained when

$$k = \frac{\pi}{\sqrt{2}}, \tag{3.22}$$

and the resulting critical value of the Rayleigh number is

$$Ra_c = \frac{27\pi^4}{4} \approx 657.5; \tag{3.23}$$

That is, the steady state is linearly unstable if $Ra > Ra_c$.

For other boundary conditions, the solutions are still exponentials, but the coefficients, and hence also the growth rate, must be found numerically. The resultant critical value of the Rayleigh number is higher for no slip boundary conditions, for example, (it is about 1707), and in general, thermal convection is initiated at values of $Ra \gtrsim O(10^3)$.

3.5 High Rayleigh number convection

We have seen that convection occurs if the Rayleigh number is larger than $O(10^3)$ in general, depending on the precise boundary conditions which apply. In the Earth's mantle, suitable values of the constituent parameters are $\alpha = 3 \times 10^{-5}$ K^{-1}, $\Delta T =$ 3000 K, $\rho_0 = 3 \times 10^3$ kg m^{-3}, $g = 10$ m s^{-2}, $d = 3000$ km, $\eta_0 = 10^{21}$ Pa s, $\kappa_0 = 10^{-6}$ m^2 s^{-1}, and for these values, the Rayleigh number is slightly less than 10^8. Thus the Rayleigh number is much larger than the critical value, and as a consequence we can expect the convection to be vigorous (if velocities of centimetres per year can be said to be vigorous).

There are various intuitive ways in which we can get a sense of the likely behaviour of the convective solutions of the Boussinesq equations when $Ra \gg 1$. Since Ra multiplies the buoyancy term, any $O(1)$ lateral temperature gradient will cause enormous velocities. One might thus expect the flow to organise itself so that either horizontal temperature gradients are small, or they are confined to thin regions, or both. Since $O(1)$ temperature variations are enforced by the boundary conditions, the latter is more plausible, and thus we have the idea of the *thermal plume*, a localised upwelling of hot fluid which will be instantly familiar to glider pilots and seabirds.

A mathematically intuitive way of inferring the same behaviour follows from the expectation that increasing Ra drives increasing velocities; then large Ra should imply large velocity, and the conduction term in the heat equation $\mathbf{u}.\boldsymbol{\nabla} T = \nabla^2 T$ is correspondingly small. Since the conduction term represents the highest derivative in the equation, its neglect would imply a reduction of order, and correspondingly we would expect *thermal boundary layers* to exist at the boundaries of the convecting cell. This is in fact what we will find: a hot thermal boundary layer adjoins the lower boundary, and a cold one adjoins the upper boundary, and a rapid circulation in the interior of the cell detaches these as upwelling and downwelling plumes. The general structure of the resulting flow is shown in figure 3.7. We analyse this structure in the following sections.

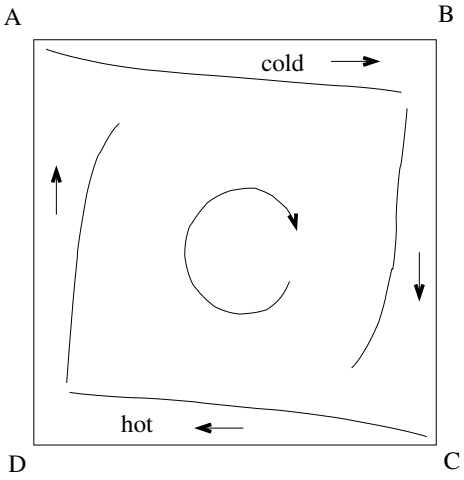

Figure 3.7: Schematic representation of boundary layer convection

3.5.1 Boundary layer theory

We now consider a convecton cell in a finite box, as shown in figure 3.7, with (dimensionless) top and bottom boundaries at $z = 0, 1$, and side walls at $x = 0, a$. The Boussinesq equations describing thermal convection are written in the following dimensionless form:

$$\begin{aligned} \boldsymbol{\nabla}.\mathbf{u} &= 0, \\ \frac{1}{Pr}\frac{d\mathbf{u}}{dt} &= -\boldsymbol{\nabla}p + \nabla^2\mathbf{u} + Ra\,T\mathbf{k}, \\ \frac{dT}{dt} &= \nabla^2 T, \end{aligned} \tag{3.24}$$

where $\mathbf{u}$ is velocity, p is pressure, T is temperature, and the Rayleigh and Prandtl numbers are defined in (3.4).

By considering only two-dimensional motion in the (x, z) plane, we define the stream function ψ by

$$u = -\psi_z, \quad w = \psi_x; \tag{3.25}$$

the vorticity is then $(0, \omega, 0)$, where $\omega = -\nabla^2\psi$. Taking the curl of the momentum equation, we derive the set

$$\begin{aligned} \omega &= -\nabla^2\psi, \\ \frac{dT}{dt} &= T_t + \psi_x T_z - \psi_z T_x = \nabla^2 T, \\ \frac{1}{Pr}\frac{d\omega}{dt} &= -Ra\,T_x + \nabla^2\omega, \end{aligned} \tag{3.26}$$

which are supplemented by the boundary conditions

$$\begin{aligned} \psi, \omega = 0 \quad &\text{on} \quad x = 0, a, \ z = 0, 1, \\ T = \tfrac{1}{2} \quad &\text{on} \quad z = 0, \\ T = -\tfrac{1}{2} \quad &\text{on} \quad z = 1, \\ T_x = 0 \quad &\text{on} \quad x = 0, a; \end{aligned} \tag{3.27}$$

here a is the aspect ratio, and we have chosen free slip (no stress) conditions at the cell boundaries. Note that we have chosen that we have changed the reference temperature for the scaled temperature from T_0 to $T_0 - \frac{1}{2}\Delta T$; this is purely a matter of convenience, as the resultant symmetry of the thermal boundary conditions is more natural.

Rescaling

The idea is that when $Ra \gg 1$, thermal boundary layers of thickness $\delta \ll 1$ will form at the edges of the flow, and both ψ and ω will be $\gg 1$ in the flow. To scale the equations properly, we rescale the variables as

$$\psi, \ \omega \sim \frac{1}{\delta^2}, \tag{3.28}$$

and define

$$\delta = Ra^{-1/3}. \tag{3.29}$$

Rescaled, the equations are thus, in the steady state,

$$\begin{aligned} \omega &= -\nabla^2 \psi, \\ \psi_x T_z - \psi_z T_x &= \delta^2 \nabla^2 T, \\ \nabla^2 \omega &= \frac{1}{\delta} T_x + \frac{1}{Pr\, \delta^2} \frac{d\omega}{dt}. \end{aligned} \tag{3.30}$$

In order that the inertia terms be unimportant, we require $Pr\, \delta^2 \gg 1$, i. e., $Pr \gg Ra^{2/3}$. This assumption is easily satisfied in the Earth's mantle, but is difficult to achieve in the laboratory. Nevertheless, we assume this henceforth.

As in any singular perturbation procedure, we now examine the flow region by region, introducing special rescalings in regions where boundary conditions cannot be satisfied. Before doing so, note that the statement of the flow problem is symmetric, and we will therefore take the solution to be symmetric also.

Core flow

The temperature equation is linear in T, and implies $T = T_0(\psi) + O(\delta^2)$. For a flow with closed streamlines, the Prandtl-Batchelor theorem then implies $T_0 =$ constant

(this follows from the exact integral $\oint_C \frac{\partial T}{\partial n} ds = 0$, where the integral is around a streamline, whence $T_0'(\psi) \oint_C \frac{\partial \psi}{\partial n} ds = 0$); it then follows that T is constant to all (algebraic) orders of δ, and is in fact zero by the symmetry of the flow. Thus

$$\begin{aligned} T &= 0, \\ \nabla^4 \psi &= 0, \end{aligned} \tag{3.31}$$

and clearly the core flow cannot have $\psi = \omega = 0$ at the boundaries, for non-zero ψ. In fact, ω jumps at the side-walls where the plume buoyancy generates a non-zero vorticity. We examine the plumes next.

Plumes

Near $x = 0$, for example, we rescale the variables as

$$x = \delta X, \quad \psi = \delta \Psi, \tag{3.32}$$

so that to leading order, we have

$$\Psi_{XX} \approx 0, \tag{3.33}$$

whence $\Psi \approx w_p(z) X$, and to match to the core flow, we define $w_p = \psi_x \,|_{x=0}$ as the core velocity at $x = 0$. Also

$$\begin{aligned} \Psi_X T_z - \Psi_z T_X &\approx T_{XX}, \\ \omega_{XX} &\approx T_X, \end{aligned} \tag{3.34}$$

the latter of which integrates to give

$$\omega = \int_0^X T \, dX, \quad \omega_p = \int_0^\infty T \, dX, \tag{3.35}$$

where matching requires ω_p to be the core vorticity at $x = 0$. Integration of $(3.34)_1$ gives

$$\int_0^\infty T \, d\Psi = C, \tag{3.36}$$

where C is constant, and it follows that the core flow must satisfy the boundary condition $\omega \psi_x = C$ on $x = 0$ (and therefore, by symmetry, $-C$ at $x = a$). In summary, the effective boundary conditions for the core flow are

$$\begin{aligned} \psi = 0 \quad &\text{on} \quad x = 0, a, \ z = 0, 1, \\ \psi_{zz} = 0 \quad &\text{on} \quad z = 0, 1, \\ \psi_x \psi_{xx} = -C \quad &\text{on} \quad x = 0, \quad \psi_x \psi_{xx} = C \quad \text{on} \quad x = a, \end{aligned} \tag{3.37}$$

and the solution can be found as the *canonical solution*

$$\psi = C^{1/2}\hat{\psi}(x, z), \tag{3.38}$$

where $\hat{\psi}$ must be determined numerically. It thus remains to determine C. This requires consideration of the thermal boundary layers. Thermal boundary layers are necessary at the top and bottom because the core temperature ($T = 0$) does not satisfy the boundary conditions there.

Thermal boundary layers

Near the top surface, for example, we rescale the variables by writing

$$z = 1 - \delta Z, \quad \psi = \delta\Psi, \quad \omega = \delta\Omega, \tag{3.39}$$

to find the leading order rescaled equation for Ψ to be simply

$$\Psi_{ZZ} \approx 0, \tag{3.40}$$

whence $\Psi \sim u_s(x)Z$, and u_s is the core value of the surface velocity $-\psi_z|_{z=1}$. Then $\Omega_{ZZ} \approx T_x$ determines Ω (with $\Omega = 0$ on $Z = 0$, and $\Omega \sim \omega_s(x)Z$ as $Z \to \infty$, where ω_s is the core value of the surface vorticity), and T satisfies

$$\Psi_Z T_x - \Psi_x T_Z \approx T_{ZZ}. \tag{3.41}$$

In Von Mises coordinates x, Ψ, the equation is

$$T_x \sim \frac{\partial}{\partial\Psi}\left[\Psi_Z \frac{\partial T}{\partial\Psi}\right], \tag{3.42}$$

and putting $\xi = \displaystyle\int_0^x u_s(x)\,dx$, this is just the diffusion equation

$$T_\xi = T_{\Psi\Psi}, \tag{3.43}$$

with

$$T = -\tfrac{1}{2} \quad \text{on} \quad \Psi = 0, \quad T \to 0 \quad \text{as} \quad \Psi \to \infty. \tag{3.44}$$

Note that the same Von Mises transformation (but from (z, X) to (z, Ψ)) can be used in the plume equation $(3.34)_1$, which can thus also be written in the diffusion equation form (3.43), where ξ is extended as $\displaystyle\int^z w_p(z)\,dz$.

A quantity of interest is the Nusselt number, defined as

$$Nu = -\int_0^1 \frac{\partial T}{\partial z}(x, 1)\,dx, \tag{3.45}$$

and from the above, this can be written as

$$Nu \approx \left[\int_0^\infty -T\,d\Psi\right]_{x=0}^{x=a} Ra^{1/3}. \tag{3.46}$$

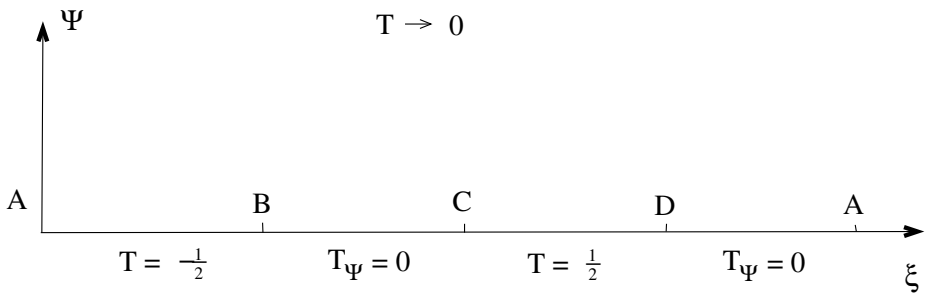

Figure 3.8: Boundary conditions for the thermal boundary layer solution of (3.49).

Corner flow

The core flow has a singularity in each corner, where (if r is distance from the corner), then $\psi \sim r^{3/2}$, $\omega \sim r^{-1/2}$, and (for the corner at $x = 0$, $z = 0$, for example) $x, z \sim r$. There must be a region where this singularity is alleviated by the incorporation of the buoyancy term. This requires $\omega/r^2 \sim 1/\delta r$, whence $r \sim \delta^{2/3}$. Rescaling the variables as indicated ($x, z \sim \delta^{2/3}$, $\psi \sim \delta$, $\omega \sim \delta^{-1/3}$) then gives the temperature equation as

$$\Psi_X T_Z - \Psi_Z T_X \sim \delta \nabla^2 T, \tag{3.47}$$

which shows that (since the ψ scale, δ, is the same as that of the boundary layers adjoining the corner) the boundary layer temperature field is carried through the corner region without change (to leading order). The corner flow thus has $T \approx T(\Psi)$, so that

$$\nabla^4 \Psi + T'(\Psi)\Psi_X = 0, \tag{3.48}$$

with appropriate matching conditions. The main point of this is to show that in solving the thermal boundary layer equations round the perimeter of the box, the transverse profile (in Ψ) can be taken to be continuous when the boundary conditions change at the corners.

Solution strategy

The Von Mises transformation shows that the temperature in the thermal boundary layers and the thermal plumes satisfies the diffusion equation

$$T_\xi = T_{\Psi\Psi}, \tag{3.49}$$

where we define

$$\xi = \int_0^s U(s)\, ds, \tag{3.50}$$

and we define s to be arc length around the perimeter of the box (starting for example at the point A in figure 3.7, and $U(s)$ is the (core-determined) tangential velocity on the perimeter. The temperature equation must be solved in the four regions

corresponding to the boundary layer at $z = 1$, plume at $x = a$, boundary layer at $z = 0$, and plume at $x = 0$, representing the four edges AB, BC, CD, DA indicated in figure 3.7, with T being continuous at each junction point (corner), and

$$\begin{aligned} T &\to 0 \quad \text{as} \quad \Psi \to \infty, \\ T &= -\tfrac{1}{2} \quad \text{on} \quad \Psi = 0 \quad [z = 1, \text{ top } AB], \\ T_\Psi &= 0 \quad \text{on} \quad \Psi = 0 \quad [x = a, \text{ right } BC], \\ T &= \tfrac{1}{2} \quad \text{on} \quad \Psi = 0 \quad [z = 0, \text{ bottom } CD], \\ T_\Psi &= 0 \quad \text{on} \quad \Psi = 0 \quad [x = 0, \text{ left } DA], \end{aligned} \tag{3.51}$$

as indicated in figure 3.8.

What of the initial condition? The novelty here is that prescription of an initial condition is supplanted by the necessary requirement that the solution be periodic in ξ. Beginning from $x = 0$, $z = 1$, we may denote the values of ξ at the corners as ξ_A ($x = 0$, $z = 1$), ξ_B ($x = a$, $z = 1$), ξ_C ($x = a$, $z = 0$), ξ_D ($x = 0$, $z = 0$). Now from the definition of ξ, we have $\xi_k = C^{1/2}\hat{\xi}_k$, where the values of $\hat{\xi}_k$ are independent of C (because they are determined by the canonical solution in (3.38)). Putting

$$\xi = C^{1/2}\hat{\xi}, \quad \Psi = C^{1/4}\hat{\Psi}, \quad T(\xi, \Psi) = \hat{T}(\hat{\xi}, \hat{\Psi}), \tag{3.52}$$

we see that the problem for $\hat{T}(\hat{\xi}, \hat{\Psi})$ is independent of C.

Just as for the flow in the core, this problem must be solved numerically for $\hat{T}(\hat{\xi}, \hat{\Psi})$. Assuming this is done, then

$$\int_0^\infty T(\xi, \Psi)\, d\Psi = C^{1/4} \int_0^\infty \hat{T}(\hat{\xi}, \hat{\Psi})\, d\hat{\Psi}. \tag{3.53}$$

If, for example, we evaluate both quantities at $\xi = 0$ (i. e., the point A), then it follows from (3.36) that

$$C = \int_0^\infty T(0, \Psi)\, d\Psi = C^{1/4} \int_0^\infty \hat{T}(0, \hat{\Psi})\, d\hat{\Psi}, \tag{3.54}$$

and this determines C as

$$C = \left[\int_0^\infty \hat{T}(0, \hat{\Psi})\, d\hat{\Psi} \right]^{4/3}. \tag{3.55}$$

Given this, the Nusselt number is then given from (3.46) as

$$Nu \approx C^{1/4} \left[-\int_0^\infty \hat{T}\, d\hat{\Psi} \right]_0^{\hat{\xi}_A} Ra^{1/3}. \tag{3.56}$$

No-slip boundary conditions

For no slip boundary conditions, the necessary preliminary rescaling is $\psi \sim 1/\delta^3$, $\omega \sim 1/\delta^3$, where $\delta = Ra^{-1/5}$. Thus the Nusselt number $Nu \sim Ra^{1/5}$. There is no longer parity between the thermal boundary layers and plumes, as the former are slowed down by the no slip conditions. The rescaled equations are

$$\begin{aligned} \omega &= -\nabla^2\psi, \\ \psi_x T_z - \psi_z T_x &= \delta^3 \nabla^2 T, \\ \nabla^2\omega &= \frac{1}{\delta^2} T_x. \end{aligned} \tag{3.57}$$

The core flow is as before; the thermal boundary layers have $\psi \sim \delta^2$, $\omega \sim 1$, $z \sim \delta$, so that vorticity balances buoyancy), and all three equations are necessary to solve for T; it is still the case that $\int T\, d\psi$ is conserved at corners, but now in the plume, $x \sim \delta^{3/2}$, $\psi \sim \delta^{3/2}$, and $T \sim \delta^{1/2}$. The initial plume profile is effectively a delta function, and the plume temperature is just the resultant similarity solution. The remainder of the structure must be computed numerically.

3.6 Double-diffusive convection

Double-diffusive convection refers to the motion which is generated by buoyancy, when the density depends on two diffusible substances or quantities. The simplest examples occur when salt solutions are heated; then the two diffusing quantities are heat and salt. Double-diffusive processes occur in sea water and in lakes, for example. Other simple examples occur in multi-component fluids containing more than one dissolved species; convection in magma chambers is one such.

The guiding principle behind double-diffusive convection is still that light fluid rises, and convection occurs in the normal way (the direct mode) when the steady state is statically unstable (i. e., when the density increases with height), but confounding factors arise when, as normally the case, the two substances diffuse at different rates. Particularly when we are concerned with temperature and salt, the ratio of thermal to solutal diffusivity is large, and in this case different modes of convection occur near the statically neutral buoyancy state: the cells can take the form of long thin 'fingers', or the onset of convection can be oscillatory. In practice, fingers are seen, but oscillations are not.

A further variant on Rayleigh-Bénard convection arises in the form of convective layering. This is a long-lived transient form of convection, in which separately convecting layers form, and is associated partly with the high diffusivity ratio, and partly with the usual occurrence of no flux boundary conditions for diffusing chemical species.

We pose a model for double-diffusive convection based on a density which is related linearly to temperature T and salt composition c in the form

$$\rho = \rho_0[1 - \alpha(T - T_0) + \beta(c - c_0)], \tag{3.58}$$

where we take α and β to be positive constants; thus the presence of salt makes the fluid heavier. The equation that then needs to be added to (3.1) is that for convective diffusion of salt:

$$c_t + \mathbf{u}.\boldsymbol{\nabla} c = D\nabla^2 c, \tag{3.59}$$

where D is the solutal diffusion coefficient, assuming a dilute solution. We adopt the same scaling of the variables as before, with the extra choice

$$c - c_0 \sim \Delta c, \tag{3.60}$$

where Δc is a relevant salinity scale (in our stability analysis, it will be the prescribed salinity difference between the lower and upper surfaces of the fluid layer). The Boussinesq form of the scaled equations, based on the assumptions that $\alpha \Delta T \ll 1$ and $\beta \Delta c \ll 1$, are then

$$\begin{aligned} \boldsymbol{\nabla}.\mathbf{u} &= 0, \\ \frac{1}{Pr}[\mathbf{u}_t + (\mathbf{u}.\boldsymbol{\nabla})\mathbf{u}] &= -\boldsymbol{\nabla} p + \nabla^2 \mathbf{u} + Ra\, T\hat{\mathbf{k}} - Rs\, c\hat{\mathbf{k}}, \\ T_t + \mathbf{u}.\boldsymbol{\nabla} T &= \nabla^2 T, \\ c_t + \mathbf{u}.\boldsymbol{\nabla} c &= \frac{1}{Le}\nabla^2 c. \end{aligned} \tag{3.61}$$

The Rayleigh number Ra and the Prandtl number Pr are defined as before, and the solutal Rayleigh number Rs and the Lewis number Le are defined by

$$Rs = \frac{\beta \rho_0 \Delta c g d^3}{\mu \kappa}, \quad Le = \frac{\kappa}{D}. \tag{3.62}$$

Note that in the absence of temperature gradients, the quantity $-Rs\, Le$ would be the effective Rayleigh number determining convection.

3.6.1 Linear stability

Now we study the linear stability of a steady state maintained by prescribed temperature and salinity differences ΔT and Δc across a stress-free fluid layer. In dimensionless terms, we pose the boundary conditions

$$\begin{aligned} \psi = \nabla^2 \psi = 0 \quad \text{at} \quad z = 0, 1, \\ T = c = 0 \quad \text{at} \quad z = 1, \\ T = c = 1 \quad \text{at} \quad z = 0, \end{aligned} \tag{3.63}$$

where as before, we restrict attention to two dimensions, and adopt a stream function ψ. The steady state is

$$c = 1 - z, \quad T = 1 - z, \quad \psi = 0, \tag{3.64}$$

and we perturb it by writing

$$c = 1 - z + C, \quad T = 1 - z + \theta, \tag{3.65}$$

and then linearising the equations on the basis that $C, \theta, \psi \ll 1$. This leads to

$$\begin{aligned} \frac{1}{Pr}\nabla^2\psi_t &\approx Ra\,\theta_x - Rs\,C_x + \nabla^4\psi, \\ \theta_t - \psi_x &\approx \nabla^2\theta, \\ C_t - \psi_x &\approx \frac{1}{Le}\nabla^2 C, \end{aligned} \tag{3.66}$$

with

$$C = \psi = \psi_{zz} = \theta = 0 \quad \text{on} \quad z = 0, 1. \tag{3.67}$$

By inspection, solutions satisfying the temperature and salinity equations are

$$\begin{aligned} \psi &= \exp(ikx + \sigma t)\sin m\pi z, \\ \theta &= \frac{ik}{\sigma + K^2}\exp(ikx + \sigma t)\sin m\pi z, \\ C &= \frac{ik}{\sigma + \dfrac{K^2}{Le}}\exp(ikx + \sigma t)\sin m\pi z, \end{aligned} \tag{3.68}$$

where we have written

$$K^2 = k^2 + m^2\pi^2. \tag{3.69}$$

Substituting these into the momentum equation leads to the dispersion relation determining σ in terms of k:

$$(\sigma + K^2 Pr)(\sigma + K^2)\left(\sigma + \frac{K^2}{Le}\right) + k^2 Pr\left[\frac{(Rs - Ra)\sigma}{K^2} + Rs - \frac{Ra}{Le}\right] = 0. \tag{3.70}$$

This is a cubic in σ, which can be written in the form

$$\sigma^3 + a\sigma^2 + b\sigma + c = 0, \tag{3.71}$$

where

$$\begin{aligned} a &= K^2\left(Pr + 1 + \frac{1}{Le}\right), \\ b &= K^4\left(Pr + \frac{1}{Le} + \frac{Pr}{Le}\right) + \frac{k^2}{K^2}Pr(Rs - Ra), \\ c &= \frac{K^6}{Le}Pr + k^2 Pr\left(Rs - \frac{Ra}{Le}\right). \end{aligned} \tag{3.72}$$

Instability occurs if any one of the three roots of (3.71) has positive real part. Since Le and Pr are properties of the fluid, we take them as fixed, and study the

effect of varying Ra and Rs on the stability boundaries where $\mathrm{Re}\,\sigma = 0$. Firstly, if $Ra < 0$ and $Rs > 0$, then a, b and c are all positive. We can then show (see question 3.3) that $\mathrm{Re}\,\sigma < 0$ for all three roots providing $ab > c$, and this is certainly the case if $Le > 1$, which is always true for heat and salt diffusion. Thus when both temperature and salinity fields are stabilising, the state of no motion is linearly stable.

To find regions of instability in the (Rs, Ra) plane, it thus suffices to locate the curves where $\mathrm{Re}\,\sigma = 0$. There are two possibilities. The first is referred to as exchange of stability, or the direct mode, and occurs when $\sigma = 0$. From (3.71), this is when $c = 0$, or $Rs = \dfrac{Ra}{Le} - \dfrac{K^6}{k^2 Le}$. This is a single curve (for each k), and since we know that $\mathrm{Re}\,\sigma < 0$ in $Ra < 0$ and $Rs > 0$, this immediately tells us that a direct instability occurs if

$$Ra - Le\,Rs > R_c = \min_k \frac{K^6}{k^2} = \frac{27\pi^4}{4}. \tag{3.73}$$

This direct transition is the counterpart of the onset of Rayleigh-Bénard convection, and shows that $Ra - Le\,Rs$ is the effective Rayleigh number. This is consistent with the remark just after (3.62).

The other possibility is that there is a Hopf bifurcation, i. e., a pair of complex conjugate values of σ cross the imaginary axis at $\pm i\Omega$, say. The condition for this is $ab = c$, which is again a single curve, and one can show (see question 3.4) that oscillatory instability occurs for

$$Ra > \frac{\left(Pr + \dfrac{1}{Le}\right) Rs}{1 + Pr} + \frac{\left(1 + \dfrac{1}{Le}\right)\left(Pr + \dfrac{1}{Le}\right)}{Pr} R_c. \tag{3.74}$$

Direct instability occurs along the line XZ in figure 3.9, while oscillatory instability occurs at the line XW. Between XW and the continuation XU of XZ, there are two roots with positive real part and one with negative real part. As Ra increases above XW, it is possible that the two complex roots coalesce on the real axis, so that the oscillatory instability is converted to a direct mode. One can show (see question 3.5) that the criterion for this is that $b < 0$ and

$$c = \tfrac{1}{9}\left[ab + \frac{(a^2 - 6b)}{3}\left\{-a + (a^2 - 3b)^{1/2}\right\}\right]. \tag{3.75}$$

For large Rs, this becomes (for $k^2 = \dfrac{\pi^2}{2}$)

$$Ra \approx Rs + \frac{3 R_c^{1/3} Rs^{2/3}}{2^{2/3} Pr^{1/3}}, \tag{3.76}$$

and is shown as the line XW in figure 3.9. Thus the onset of convection is oscillatory only between the lines XW and XV, and beyond (above) XV it is direct. In practice, oscillations are rarely seen.

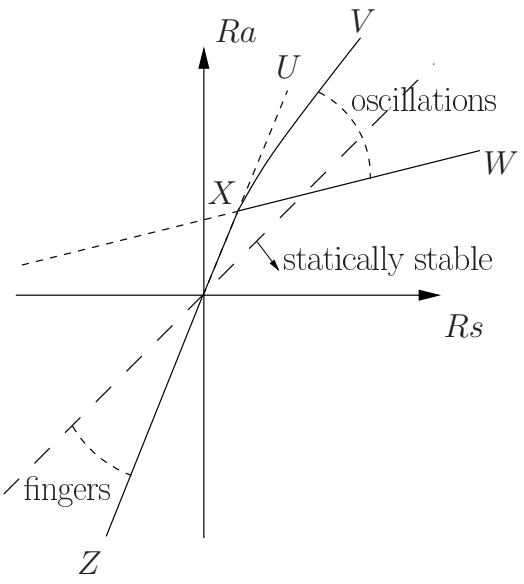

Figure 3.9: Stability diagram for double-diffusive convection.

Fingers

If we return to the cubic in the form (3.70), and consider the behaviour of the roots in the third quadrant as $Ra, Rs \to -\infty$, it is easy to see that one root is

$$\sigma \approx \frac{K^2 \left[\dfrac{Ra}{Le} - Rs \right]}{Rs - Ra}, \tag{3.77}$$

while the other two are oscillatorily stable (see question 3.6). Thus this growth rate is positive when $Le\, Rs < Ra < Rs$ and grows unboundedly with the wave number k (since $K^2 = k^2 + \pi^2$ when $m = 1$). This is an indication of ill-posedness, and in fact we anticipate that σ will become negative at large k. To see when this occurs, inspection of (3.70) shows that the neglected terms in the approximation (3.77) become important when $k \sim |Ra|^{1/4}$, where σ is maximum (of $O|Ra|^{1/2}$), and then $\sigma \sim -O(k^2)$ for larger k.[2] Thus in the 'finger' régime sector indicated in figure 3.9, the most rapidly growing wavelengths are short, and the resulting waveforms are tall and thin. This is what is seen in practice, and the narrow cells are known as fingers. An example is shown in figure 3.10.

3.6.2 Layered convection

The linear stability analysis we have given above is only partially relevant to double diffusive convection. It is helpful in the understanding of the finger régime, but

[2] In the common case where $Pr, Le > 1$, one finds $\sigma \approx -\dfrac{k^2}{Le}$.

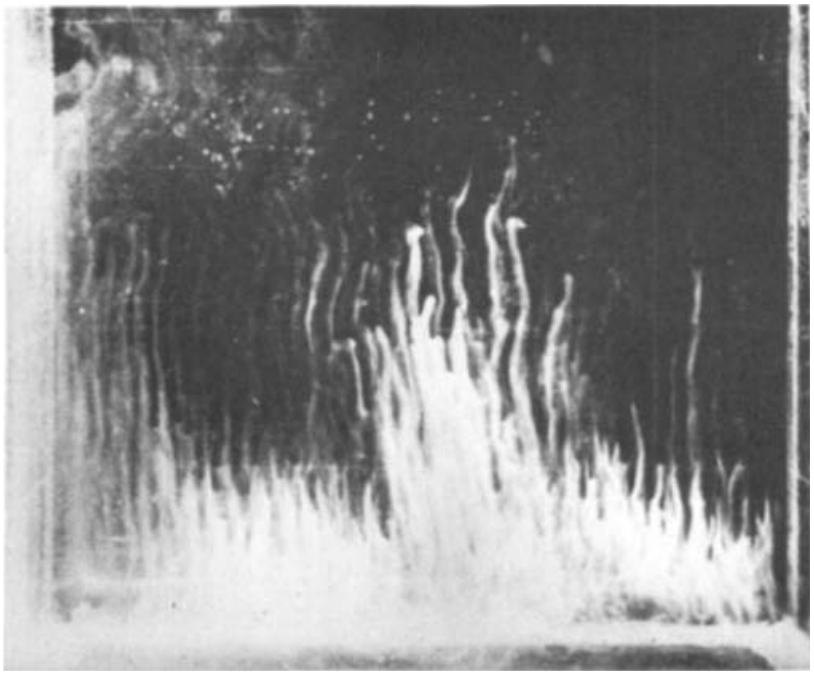

Figure 3.10: Finger convection (Turner 1974).

the oscillatory mode of convection is not particularly relevant. The other principal phenomenon which double diffusive systems exhibit is that of layering. This is a transient, but long-term, phenomenon associated often with the heating of a stable salinity gradient, and arises because in normal circumstances, more appropriate boundary conditions for salt concentration are to suppose that there is no flux at the bounding surfaces.

In pure thermal convection, the heating of an initially stably thermally stratified fluid will lead to the formation of a layer of convecting fluid below the stable region. This (single) convecting layer will grow in thickness until it fills the entire layer. This is essentially the 'filling box'. Suppose now we have a stable salinity gradient which is heated from below. Again a convecting layer forms, which mixes the temperature and concentration fields so that they are uniform within the layer. At the top of the convecting layer, there will be a step down ΔT in temperature, and a step down Δc in salinity. It is found experimentally that $\alpha\Delta T = \beta\Delta c$, that is, the *boundary layer*[3] is neutrally stable. However, the disparity in diffusivities (typically $Le \gg 1$) means that there is a thicker thermal conductive layer ahead of the interface. In effect, the stable salinity gradient above the convecting layer is heated by the layer itself, and a second, and then a third, layer forms. In this way, the entire fluid depth can fill up with a sequence of long-lived, separately convecting layers. The layers will eventually merge and form a single convecting layer over a time scale controlled by the very slow transport of salinity between the convecting layers. Such layers are very suggestive

[3]For discussion of boundary layers, see section 3.5.1.

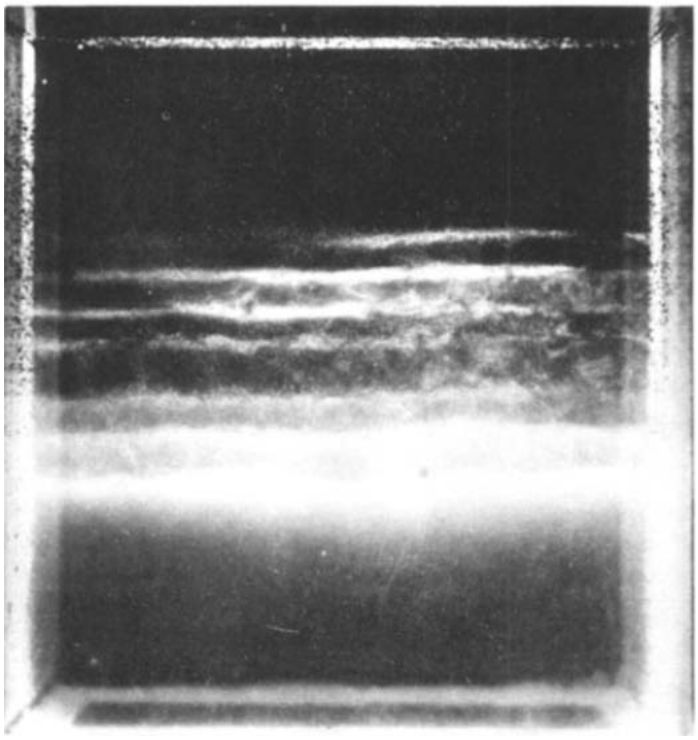

Figure 3.11: Layered convection (Turner 1974). A stable salt solution has been heated from below.

of some of the fossilised layering seen in magma chambers, as for example in figure 3.5, but the association may be a dangerous one. An experimental realisation of this form of layered convection is shown in figure 3.11.

A further example of some of the exotic behaviour which double diffusion can lead to is shown in figure 3.12, again taken from the review article by Turner (1974). In this experiment, the two diffusing substances were sugar and salt, and the fluid was initially set up with a top-heavy gradient of salt (which plays the rôle of temperature here as its diffusivity is larger) and a bottom-heavy gradient of sugar, such that the overall density gradient was statically stable. This is the analogue of cold/fresh above hot/salty, so in the 'diffusive' régime of the first quadrant in figure 3.9. The rôle of the Prandtl number is taken by the Schmidt number defined by

$$Sc = \frac{\nu}{D_l}, \tag{3.78}$$

where D_l is the diffusivity of salt and ν is the kinematic viscosity. (The 'Lewis' number is the ratio D_l/D_g, where D_g is the diffusivity of sugar. For salt and sugar, $Le \approx 3.$[4]) Now the Schmidt number for salt is around 10^6, so the 'Prandtl' number is large, and the static stability limit in the diffusive régime is essentially the same as the

[4]Specifically, $D_l \approx 1.5 \times 10^{-9}$ m^2 s^{-1} (Vitagliano and Lyons 1956) and $D_g \approx 0.5 \times 10^{-9}$ m^2 s^{-1} (Ziegler *et al.* 1987).